

# **Nonlinear pseudo-force in “breathing” delamination to generate harmonics: A mechanism and application study**

**Maosen Cao<sup>a, b</sup>, Zhongqing Su<sup>c</sup>, Tongfa Deng<sup>a</sup>, Wei Xu<sup>a, c, b, \*</sup>**

<sup>a</sup> Jiangxi Provincial Key Laboratory of Environmental Geotechnical Engineering and Disaster Control, Jiangxi University of Science and Technology, Ganzhou 341000, People’s Republic of China

<sup>b</sup> Department of Engineering Mechanics, Hohai University, Nanjing 210098, People’s Republic of China

<sup>c</sup> Department of Mechanical Engineering, The Hong Kong Polytechnic University, Hung Hom, Kowloon, Hong Kong, People’s Republic of China

---

\*Corresponding author.

*E-mail addresses:* cmszhy@hhu.edu.cn (M. Cao); zhongqing.su@polyu.edu.hk (Z. Su); tfdeng@jxust.edu.cn (T. Deng); wxu@hhu.edu.cn, weixu@polyu.edu.hk (W. Xu);

**Abstract:** Subject to coupled vibro-acoustic excitation, the opening–closing motion of a “breathing” delamination in a composite laminate can create nonlinear harmonics, *i.e.*, higher and sideband harmonics, in its steady-state vibration responses. Nonlinear harmonics have attracted increasing attention in the field of nondestructive testing because they can be sensitive indicators of barely visible delamination that is difficult to detect by conventional linear approaches. Although vibro-acoustic modulation has been acknowledged as the cause of nonlinear harmonics, the intrinsic force in a delamination that generates harmonics is not yet clear. Addressing this problem, this study analytically formulates a novel concept of nonlinear pseudo-force (NPF) in “breathing” delamination of composite laminates, by which the mechanism for generating nonlinear harmonics by vibro-acoustic modulation can be explicitly expounded. In the application aspect, as the NPF in delamination can cause local changes in operating deflection shapes (ODSs), this study proposes a novel approach using ODSs at nonlinear harmonics for locating “breathing” delamination of composite laminates, which is superior to current approaches that can only manifest the occurrence of delamination by nonlinear harmonics. Numerical simulations using finite element method are used to validate the mechanism and explore the application potential of ODSs for locating delamination. In particular, an array of coupled vibro-acoustic excitation is proposed to avoid wave attenuation of acoustic excitations. Thereby, vibration and acoustics can interact in the “breathing” delamination to generate nonlinear harmonics.

**Keywords:** “breathing” delamination; nonlinear pseudo-force; nonlinear harmonic; vibro-acoustic modulation; operating deflection shape; delamination localization

## 1. Introduction

The nonlinear vibration behavior of “breathing” delamination is a classical and interesting problem with applications in identifying delamination in composite laminates [1]. Superior to the “constrained mode” delamination theory [2], in which delaminated layers always have identical transverse vibration deflections, delaminated layers of “breathing” delamination are allowed to contact and separate to produce the opening–closing motion of the delamination as observed in experiments [3]. Contacts between delamination interfaces occur when “breathing” delaminations close [4-8] and vanish when “breathing” delaminations open. In the open state, “free mode” delamination theory [9] can be utilized to separately depict vibration of the delaminated layers.

Subject to the coupled vibro-acoustic excitation that consists of low- and high-frequency harmonic excitations, steady-state vibration responses of a composite laminate that bears a delamination can be nonlinear, owing to opening–closing motion of the delamination. For an open delamination that is always open during vibration, responses can be decomposed into corresponding low- and high-frequency harmonics (referred to as linear harmonics); in contrast, for a “breathing” delamination that periodically opens and closes during vibration, higher and sideband harmonics (referred to as nonlinear harmonics) appear, except for linear harmonics [10]. As delamination-caused nonlinear harmonics can be sensitive indicators of barely visible delaminations that are difficult to detect by conventional linear approaches, increasing attention has been focused on nonlinear harmonics for nondestructive testing (NDT) of composite laminates. In the past two decades, research on delamination-caused nonlinear harmonics can be divided into three aspects, from phenomenon to mechanism and thence to application.

**Phenomenon aspect:** Since the phenomenon of sideband harmonics accompanying forced nonlinear vibrations was reported in 1966 [11], increasing attention has been paid to nonlinear harmonics with applications in the field of NDT. In 1998, a new nonlinearity called contact acoustic nonlinearity (CAN) was observed, caused by normal stress in contact (nonbounded) interfaces for “clapping” and “rubbing” vibration patterns, by which higher and sideband harmonics could be produced [12]. In 2000, the concept of nonlinear elastic wave spectroscopy (NEWS) associated with delamination-induced higher and sideband harmonics was established [13,14].

**Mechanism aspect:** Solodov *et al.* [15] proposed the theory that CAN is assumed to be concerned with stiffness asymmetry, forming a “bimodular” model: due to the weakening of the contact between the surfaces, the compression elasticity is higher than that for a tensile stress. Van Den Abeele *et al.* [13] proposed the theory of nonlinear mesoscopic elasticity to explain nonlinear behavior, using a simplified one-dimensional model with a nonlinear stress-strain relationship. Linear, nonlinear classical, and nonlinear hysteretic models were presented for comparisons. This theory and its models were applied to composite structures with impact damage [16]. Modulation of acoustics by vibration has been acknowledged as the mechanism for generating nonlinear harmonics. In Ref [17], it was assumed that the displacement response of a delaminated laminate is a linear combination of linear and nonlinear harmonics. Force components at corresponding frequencies were considered to produce such displacement components. Linear vibrations are linearly produced by external excitations, whereas nonlinear vibrations are produced by nonlinear forces in delamination [18,19].

**Application aspect:** Solodov [12] used ultrasonic waves propagating on interfaces to exhibit the CAN, by which several modes of nonlinear NDT were proposed for the detection of small fractured defects that were almost “invisible” by linear NDT

techniques. Solodov [20] excited delaminated composite laminates in the vicinity of higher harmonics to enhance nonlinear air-coupled emission, whereby delamination could be detected and imaged for nondestructive evaluation. Through observation of the occurrence of higher and sideband harmonics in the response spectrum subject to coupled vibro-acoustic excitation, NEWS techniques were widely developed to manifest the occurrence of delamination [13,14,16,21]. In the past decade, most attention has been focused on modern sensing techniques for identifying delamination in composite laminates [22-29]. It is noteworthy that the local defect resonance (LDR) discovered by Solodov [30] has been found useful for stimulating nonlinearities.

Although intensive efforts have been made to investigate vibro-acoustic modulation of “breathing” delamination, the intrinsic force in a delamination that generates harmonics is not yet clear. Addressing this problem, this study analytically formulates a novel concept of nonlinear pseudo-force (NPF) in “breathing” delamination, by which the mechanism for generating nonlinear harmonics by vibro-acoustic modulation is explicitly expounded. In the application aspect, as the NPF in delamination can cause local changes in operating deflection shapes (ODSs), this study proposes a novel approach using ODSs at nonlinear harmonics for locating “breathing” delamination of composite laminates, which is superior to current approaches that can only manifest the occurrence of delamination by nonlinear harmonics.

The rest of this paper is organized as follows. Section 2 formulates the concept of NPF in a “breathing” delamination that drives vibro-acoustic modulation, by which the analytical mechanism of generating nonlinear harmonics is explicitly expounded. Section 3 numerically verifies the nonlinear harmonics generated by “breathing” delamination using the finite element (FE) method. Section 4 proposes a novel approach

using ODSs at nonlinear harmonics to locate “breathing” delamination. Section 5 presents concluding remarks.

## 2. Mechanism for generating harmonics by NPF in “breathing” delamination

### 2.1 NPF in “breathing” delamination

The nonlinear constitutive (*i.e.*, stress-strain) relations of “breathing” delamination in composite laminates have usually been represented using a simplified one-dimensional model. In this study, to model realistic “breathing” delamination in composite laminates, a fiber reinforced cross-ply laminate made of 0/90° orientations is considered, each thin ply of which can be regarded as homogeneous and orthotropic. The constitutive equations for an element in the  $d$ th ply can be expressed as [31]

$$\begin{bmatrix} \sigma_x \\ \sigma_y \\ \tau_{xy} \end{bmatrix}_d = \begin{bmatrix} \bar{Q}_{11} & \bar{Q}_{12} & 0 \\ \bar{Q}_{12} & \bar{Q}_{22} & 0 \\ 0 & 0 & \bar{Q}_{66} \end{bmatrix}_d \begin{bmatrix} \varepsilon_x \\ \varepsilon_y \\ \gamma_{xy} \end{bmatrix}_d, \quad (1)$$

where stresses ( $\sigma_x$ ,  $\sigma_y$ , and  $\tau_{xy}$ ) and strains ( $\varepsilon_x$ ,  $\varepsilon_y$ , and  $\gamma_{xy}$ ) are in the global coordinate, and  $\bar{Q}_{ij}$  with  $i=1,2,6$  and  $j=1,2,6$  are the corresponding material constants, as can be found in Ref. [31].

By integrating stresses over the cross-section of the laminate, one can obtain the bending moments  $M_x$  and  $M_y$  and the twisting moment  $M_{xy}$ :

$$\begin{bmatrix} M_x \\ M_y \\ M_{xy} \end{bmatrix} = \begin{bmatrix} D_{11} & D_{12} & 0 \\ D_{12} & D_{22} & 0 \\ 0 & 0 & D_{66} \end{bmatrix} \begin{bmatrix} \kappa_x \\ \kappa_y \\ 2\kappa_{xy} \end{bmatrix}, \quad (2)$$

where  $D_{ij} = \frac{1}{3} \sum_{d=1} \bar{Q}_{ij}^{(d)} (z_d^3 - z_{d-1}^3)$  are stiffness coefficients integrated ply-wise over the

thickness, and  $z_d$  is the distance from the middle surface to the surface of the  $d$ th ply

having the furthest  $z$ -coordinate;  $\kappa_x = \frac{\partial^2 w}{\partial x^2}$  and  $\kappa_y = \frac{\partial^2 w}{\partial y^2}$  are the curvatures, and

$\kappa_{xy} = \frac{\partial^2 w}{\partial x \partial y}$  is the twist in the midsurface, with  $w(x, y, t)$  being the out-of-plane

displacement.

For a laminate bearing an open delamination whose interfaces do not contact each other during vibration, the equation of motion subject to coupled vibro-acoustic excitation can be expressed as

$$D_{11} \frac{\partial^4 w}{\partial x^4} + 2(D_{12} + 2D_{66}) \frac{\partial^4 w}{\partial x^2 \partial y^2} + D_{22} \frac{\partial^4 w}{\partial y^4} + \bar{\rho} \frac{\partial^2 w}{\partial t^2} + c \frac{\partial w}{\partial t} = f_L + f_H, \quad (3)$$

where  $\bar{\rho} = \sum_{d=1} \rho^{(d)} (z_d - z_{d-1})$  is the average mass density of the plate per unit area of

the midsurface with  $\rho^{(d)}$  the density of the  $d$ th lamina per unit volume,  $c$  is the damping coefficient,  $f_L(t)$  and  $f_H(t)$  are low- and high-frequency harmonic excitations with angular frequencies  $\omega_L$  and  $\omega_H$ , respectively, to constitute the

coupled vibro-acoustic excitation. **Note that for a plate made of isotropic materials such as metallic materials, its stiffness coefficients become  $D_{11}=D_{22}=D$ ,  $D_{12}=\nu D$ , and**

**$D_{66} = \frac{1-\nu}{2} D$  with the flexural rigidity  $D = \frac{Eh^3}{12(1-\nu^2)}$ , in which  $E$ ,  $h$ , and  $\nu$  are**

**the elastic modulus, plate thickness, and Poisson's ratio, respectively.** Considering a

composite laminate bearing an open delamination whose region is denoted as  $\Omega$ , the

stiffness coefficients  $D_{ij}(x, y)$  of the laminate can be represented as

$$D_{ij}(x, y) = \begin{cases} D_{ij}^I & x, y \notin \Omega \\ D_{ij}^D(x, y) & x, y \in \Omega \end{cases}, \quad (4)$$

where  $D_{ij}^I$  and  $D_{ij}^D$  are the stiffness coefficients under the intact and delaminated statuses, respectively. By substituting Eq. (4) into Eq. (3) and rearranging Eq. (3), one can obtain

$$D_{11}^I \frac{\partial^4 w}{\partial x^4} + 2(D_{12}^I + 2D_{66}^I) \frac{\partial^4 w}{\partial x^2 \partial y^2} + D_{22}^I \frac{\partial^4 w}{\partial y^4} + \bar{\rho} \frac{\partial^2 w}{\partial t^2} + c \frac{\partial w}{\partial t} = f_L + f_H + f_{LPF}, \quad (5)$$

where  $f_{LPF}(x, y, t)$  is the equivalent force caused by the open delamination, defined as the linear pseudo-force (LPF) because the vibration is linear:

$$f_{LPF} = \begin{cases} 0 & x, y \notin \Omega \\ \Delta \mathbf{D} \cdot \Theta(w) & x, y \in \Omega \end{cases}, \quad (6)$$

with  $\Delta \mathbf{D} = (D_{11}^I - D_{11}^D, (D_{12}^I + 2D_{66}^I) - (D_{12}^D + 2D_{66}^D), D_{22}^I - D_{22}^D)$  denoting the stiffness

change vector, and  $\Theta(\square) = (\frac{\partial^4}{\partial x^4}, \frac{2\partial^4}{\partial x^2 \partial y^2}, \frac{\partial^4}{\partial y^4})$ . It is noted the LPF in Eq. (6) is

equivalent to the concept of damage-caused force for delamination in the authors' previous work [32].

In contrast to an open delamination, a “breathing” delamination opens and closes periodically subject to harmonic excitations, and contact between the delamination interfaces occurs during the closing process. The frequency of the periodical opening-closing motion of the “breathing” delamination is defined as the “breathing” frequency in this study, denoted as  $\omega_B$ . As per linear vibration theory,  $f_L$  and  $f_H$  produce periodical tension and compression in the delamination at  $\omega_L$  and  $\omega_H$ , respectively, therefore both  $\omega_L$  and  $\omega_H$  can be the potential “breathing” frequency  $\omega_B$ .

The constitutive relation in the delamination region has usually been simplified in a one-dimensional form to represent the nonlinearity [13]:

$$\sigma = \int K(\varepsilon, \dot{\varepsilon}) d\varepsilon, \quad (7)$$

in which  $\dot{\varepsilon}$  is the strain rate and  $K$  is the nonlinear and hysteretic modulus given by

$$K(\varepsilon, \dot{\varepsilon}) = K_0 \{1 - \beta \varepsilon - \delta \varepsilon^2 + \alpha [\Delta \varepsilon + \varepsilon(t) \text{sign}(\dot{\varepsilon})] + \dots\}, \quad (8)$$

where  $K_0$  is the linear modulus,  $\beta$  and  $\delta$  are classical nonlinear perturbation coefficients,  $\alpha$  is a measure of the material hysteresis, and  $\Delta \varepsilon$  is the local strain amplitude over the previous period. For the 1st order classical nonlinearity with  $\delta = 0$  and  $\alpha = 0$ , the modulus  $K$  becomes asymmetric for tension and compression, periodically changing from  $K^c$  when the delamination is totally closed to  $K^o$  when the delamination is totally open (illustrated in Fig. 1 with the “breathing” period  $T = 2\pi / \omega_B$ ).

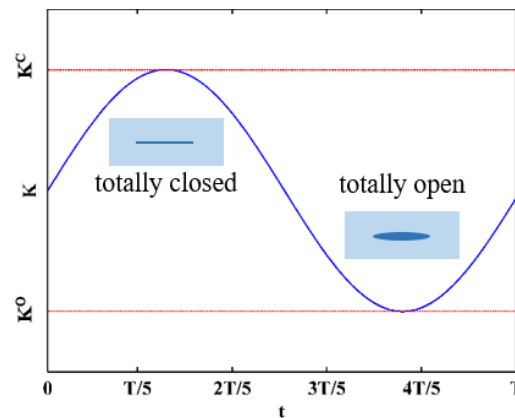


**Fig. 1.** Modulus of “breathing” delamination versus time over a “breathing” period (the modulus reaches its maximum and minimum when the delamination is totally closed and open, respectively).

Similar to “breathing” cracks [33-43], modulus  $K$  in “breathing” delamination can be assumed as a cosine function with respect to time [43]. Thereby, the stiffness coefficients in a composite laminate can be expressed as

$$D_{ij}(x, y) = \begin{cases} D_{ij}^c & x, y \notin \Omega \\ D_{ij}^c - \frac{1}{2}(D_{ij}^c - D_{ij}^o)(1 + \cos \omega_B t) & x, y \in \Omega \end{cases}, \quad (9)$$

where  $D_{ij}^C(x, y)$  and  $D_{ij}^O(x, y)$  represent the stiffness coefficients under the fully closed and open statuses of the delamination, respectively. Note that under the fully closed status, the laminate can be regarded as intact, leading to  $D_{ij}^C(x, y) = D_{ij}^I$ ; under the fully open status, the laminate can be regarded as delaminated, leading to  $D_{ij}^O(x, y) = D_{ij}^D(x, y)$ . By substituting Eq. (9) into Eq. (3) and rearranging Eq. (3), one can obtain

$$D_{11}^I \frac{\partial^4 w}{\partial x^4} + 2(D_{12}^I + 2D_{66}^I) \frac{\partial^4 w}{\partial x^2 \partial y^2} + D_{22}^I \frac{\partial^4 w}{\partial y^4} + \bar{\rho} \frac{\partial^2 w}{\partial t^2} + c \frac{\partial w}{\partial t} = f_L + f_H + f_{NPF}, \quad (10)$$

where  $f_{NPF}(x, y, t)$  is the equivalent force caused by the “breathing” delamination, defined as the NPF:

$$f_{NPF} = \begin{cases} 0 & x, y \notin \Omega \\ \frac{1}{2}(1 + \cos \omega_B t) \Delta \mathbf{D} \cdot \boldsymbol{\Theta}(w) & x, y \in \Omega \end{cases} \quad (11)$$

For elements in the laminate bearing no transverse excitation,  $f_L$  and  $f_H$  in Eqs. (5) and (10) vanish, regardless of delamination; on the other hand, the LPF and NPF appear in delamination regions only, reflecting local perturbations in equilibrium caused by the open and “breathing” delamination, respectively.

## 2.2 Nonlinear harmonics generated by nonlinear pseudo-force

For linear vibration, it is well known that the out-of-plane displacement  $w$  is linearly determined by  $f_L$  and  $f_H$  to produce linear harmonics at  $\omega_L$  and  $\omega_H$  with amplitudes ( $W_L$  and  $W_H$ ) and phases ( $\phi_L$  and  $\phi_H$ ), respectively:

$$w(x, t) = W_L(x) \cos(\omega_L t + \phi_L) + W_H(x) \cos(\omega_H t + \phi_H). \quad (12)$$

By substituting Eq. (12) into Eq. (6), the LPF in the delamination region consists of two components at  $\omega_L$  and  $\omega_H$  :

$$f_{LPF} = \Delta \mathbf{D} \cdot [\Theta(W_L) \cos(\omega_L t + \phi_L) + \Theta(W_H) \cos(\omega_H t + \phi_H)]. \quad (13)$$

In contrast to the linear vibration of open delamination, the nonlinear vibration of “breathing” delamination becomes much more complex, due to the periodically varying stiffness expressed in Eq. (9). As observed in experiments, besides linear harmonics at  $\omega_{L,1}$  and  $\omega_{H,1}$ , displacement responses contain higher harmonics at  $\omega_{L,m}$  and  $\omega_{H,n}$  ( $m = 2, \dots, M$ ,  $n = 2, \dots, N$ ) and sideband harmonics at  $\omega_{S_{n,\pm m}}$  ( $m = 1, \dots, M$ ,  $n = 1, \dots, N$ ) with respective amplitudes ( $W_{L,m}$ ,  $W_{H,n}$ , and  $W_{S_{n,\pm m}}$ ), angular frequencies ( $\omega_{L,m}$ ,  $\omega_{H,n}$ , and  $\omega_{S_{n,\pm m}}$ ), and phases ( $\phi_{L,m}$ ,  $\phi_{H,n}$ , and  $\phi_{S_{n,\pm m}}$ ):

$$\begin{aligned} w = & \sum_{m=1}^M W_{L,m} \cos(\omega_{L,m} t + \phi_{L,m}) + \sum_{n=1}^N W_{H,n} \cos(\omega_{H,n} t + \phi_{H,n}) \\ & + \sum_{n=1}^N \sum_{m=1}^M W_{S_{n,\pm m}} \cos(\omega_{S_{n,\pm m}} t + \phi_{S_{n,\pm m}}). \end{aligned} \quad (14)$$

It is noteworthy that the frequencies of linear harmonics correspond to excitation frequencies as per linear vibration theory, *i.e.*,  $\omega_{L,1} = \omega_L$  and  $\omega_{H,1} = \omega_H$ . Nevertheless, the theoretical frequencies of the nonlinear harmonics in Eq. (14) are unknown. By substituting Eq. (14) into Eq. (11), the NPF in the delamination region consists of three corresponding components:

$$f_{NPF} \Big|_{x,y \in \Omega} = f_{NPF,L} + f_{NPF,H} + f_{NPF,S}. \quad (15)$$

In Eq. (15),  $f_{NPF,L}$  is generated by  $W_{L,m}$ :

$$\begin{aligned}
f_{NPF,L} &= \frac{1}{2}(1 + \cos \omega_B t) \sum_{m=1}^M \Delta \mathbf{D} \cdot \Theta(W_{L,m}) \cos(\omega_{L,m} t + \phi_{L,m}) \\
&= \frac{1}{2} \sum_{m=1}^M \Delta \mathbf{D} \cdot \Theta(W_{L,m}) (X_{L,m} + X_{L,m}^+ + X_{L,m}^-),
\end{aligned} \tag{16}$$

where  $X_{L,m} = \cos(\omega_{L,m} t + \phi_{L,m})$ ,  $X_{L,m}^+ = \frac{1}{2} \cos((\omega_{L,m} + \omega_B) t + \phi_{L,m})$ ,

$X_{L,m}^- = \frac{1}{2} \cos((\omega_{L,m} - \omega_B) t + \phi_{L,m})$ . It can be seen from Eq. (16) that the

components of the NPF at  $\omega_{L,m}$  are modulated by  $\omega_B$ . When  $\omega_B$  is  $\omega_L$ , extra components at  $\omega_{L,m} \pm \omega_L$  are generated. Conversely, such extra components must generate displacements at corresponding frequencies as per linear vibration theory, leading to the relationship:

$$\omega_{L,m+1} = \omega_{L,m} + \omega_L. \tag{17a}$$

Considering that  $\omega_{L,1} = \omega_L$ ,  $\omega_{L,m}$  can be expressed as

$$\omega_{L,m} = m\omega_L. \tag{17b}$$

Similarly,  $f_{NPF,H}$  is generated by  $W_{H,n}$ :

$$\begin{aligned}
f_{NPF,H} &= \frac{1}{2}(1 + \cos \omega_B t) \sum_{n=1}^N \Delta \mathbf{D} \cdot \Theta(W_{H,n}) \cos(\omega_{H,n} t + \phi_{H,n}) \\
&= \frac{1}{2} \sum_{n=1}^N \Delta \mathbf{D} \cdot \Theta(W_{H,n}) (X_{H,n} + X_{H,n}^+ + X_{H,n}^-) \\
&\quad + \frac{1}{2} \sum_{n=1}^N \Delta \mathbf{D} \cdot \Theta(W_{H,n}) (Y_{H,n} + Y_{H,n}^+ + Y_{H,n}^-),
\end{aligned} \tag{18}$$

where  $X_{H,n} = \cos(\omega_{H,n} t + \phi_{H,n})$ ,  $X_{H,n}^+ = \frac{1}{2} \cos((\omega_{H,n} + \omega_H) t + \phi_{H,n})$ ,

$X_{H,n}^- = \frac{1}{2} \cos((\omega_{H,n} - \omega_H) t + \phi_{H,n})$  for  $\omega_B$  being  $\omega_H$ ,

$$Y_{H,n} = \cos(\omega_{H,n}t + \phi_{H,n}) \quad , \quad Y_{H,n}^+ = \frac{1}{2} \cos((\omega_{H,n} + \omega_L)t + \phi_{H,n}) \quad ,$$

$$Y_{H,n}^- = \frac{1}{2} \cos((\omega_{H,n} - \omega_L)t + \phi_{H,n}) \quad \text{for } \omega_B \text{ being } \omega_L .$$

It can be clearly seen from Eq. (18) that the components of the NPF at  $\omega_{H,n}$  are modulated by  $\omega_B$ , whereby extra components at  $\omega_{H,n} \pm \omega_H$  and  $\omega_{H,n} \pm \omega_L$  are generated respectively. Conversely, such extra components must generate displacements at corresponding frequencies, leading to the relationship:

$$\omega_{H,n+1} = \omega_{H,n} + \omega_H . \quad (19a)$$

Considering that  $\omega_{H,1} = \omega_H$ ,  $\omega_{H,n}$  can be expressed as

$$\omega_{H,n} = n\omega_H . \quad (19b)$$

On the other hand, the 1st and -1st sideband harmonics occur on both sides of  $\omega_{H,n}$ :

$$\omega_{Sn,\pm 1} = \omega_{H,n} \pm \omega_L . \quad (19c)$$

Finally,  $f_{NPF,S}$  is generated by  $W_{Sn,\pm m}$ :

$$\begin{aligned} f_{NPF,S} &= \frac{1}{2} (1 + \cos \omega_B t) \sum_{n=1}^N \sum_{m=1}^M \Delta \mathbf{D} \cdot \Theta(W_{Sn,\pm m}) \cos(\omega_{Sn,\pm m} t + \phi_{Sn,\pm m}) \\ &= \frac{1}{2} \sum_{n=1}^N \sum_{m=1}^M \Delta \mathbf{D} \cdot \Theta(W_{Sn,\pm m}) (Y_{Sn,\pm m} + Y_{Sn,\pm m}^+ + Y_{Sn,\pm m}^-), \end{aligned} \quad (20)$$

where  $Y_{Sn,\pm m} = \cos(\omega_{Sn,\pm m} t + \phi_{Sn,\pm m})$ ,  $Y_{Sn,\pm m}^+ = \frac{1}{2} \cos((\omega_{Sn,\pm m} + \omega_L)t + \phi_{Sn,\pm m})$ ,

$Y_{Sn,\pm m}^- = \frac{1}{2} \cos((\omega_{Sn,\pm m} - \omega_L)t + \phi_{Sn,\pm m})$  for  $\omega_B$  being  $\omega_L$ . From Eq. (20), it

can be seen that the components of the NPF at  $\omega_{Sn,\pm m}$  are modulated by  $\omega_B$  to

generate extra components at  $\omega_{S_n, \pm m} \pm \omega_L$ . Conversely, such extra components must generate displacements at corresponding frequencies, leading to the relationship:

$$\omega_{S_n, \pm m+1} = \omega_{S_n, \pm m} \pm \omega_L; \quad (21a)$$

considering  $\omega_{S_n, \pm 1} = \omega_{H, n} \pm \omega_L$  in Eq. (19c),  $\omega_{S_n, \pm m}$  can be expressed as

$$\omega_{S_n, \pm m} = n\omega_H \pm m\omega_L. \quad (21b)$$

Accordingly,  $f_{NPF, L}$ ,  $f_{NPF, H}$ , and  $f_{NPF, S}$  in Eq. (15) can be assumed as

follows with the respective amplitudes  $F_{L, m}$ ,  $F_{H, n}$ , and  $F_{S_n, \pm m}$ :

$$\begin{aligned} f_{NPF} \Big|_{x, y \in \Omega} = & \sum_{m=1}^M F_{L, m} \cos(\omega_{L, m} t + \phi_{L, m}) + \sum_{n=1}^N F_{H, n} \cos(\omega_{H, n} t + \phi_{H, n}) \\ & + \sum_{n=1}^N \sum_{m=1}^M F_{S_n, \pm m} \cos(\omega_{S_n, \pm m} t + \phi_{S_n, \pm m}). \end{aligned} \quad (22)$$

Actually, the NPF can degenerate into the LPF (expressed in Eq. (13)) when the “breathing” delamination becomes the open delamination:

$$f_{LPF} \Big|_{x, y \in \Omega} = F_{L, 1} \cos(\omega_{L, 1} t + \phi_{L, 1}) + F_{H, 1} \cos(\omega_{H, 1} t + \phi_{H, 1}). \quad (23)$$

Subject to coupled vibro-acoustic excitation, linear harmonics of a composite laminate bearing a “breathing” delamination are generated by the external excitations and the components of the NPF at linear harmonics, whereas its nonlinear harmonics are totally generated by the NPF at nonlinear harmonics.

Theoretical solutions to the nonlinear harmonics in Eqs. (17b), (19b), and (21b) correspond to the results observed in experiments [21-29]. By means of the above modulation, components of the NPF are coupled with displacement components to reach a steady state, whereby nonlinear harmonics are generated. Thereby, the analytical mechanism for the generation of nonlinear harmonics by vibro-acoustic modulation in “breathing” delamination is explicitly expounded. It should be noted that,

with the aim of revealing the mechanism for generating nonlinear harmonics, Eqs. (16), (18), and (20) are used to expound the coupled relationship between components of the NPF and displacement, whose closed-form solution is not given in this study. The simplified one-dimensional model of a “breathing” delamination, the solutions of nonlinear harmonics can also be obtained using series expansion of displacements [29].

### 3. Numerical verification

Nonlinear harmonics generated by “breathing” delamination have usually been observed through experiments. To comprehensively investigate such nonlinear harmonics in various scenarios of composite laminates, numerical simulations using the FE method are undertaken to model delaminated composite laminates and calculate their nonlinear vibro-acoustic responses. In this section, 8-layer carbon fiber reinforced polymer (CFRP) antisymmetric cross-ply 0/90° laminates bearing “breathing” delamination are considered as numerical specimens.

#### 3.1 Finite element modeling

Four edges of the composite laminate are clamped. As illustrated in Fig. 2, dimensions of the laminate are 200 mm × 200 mm × 5 mm in the  $x$ -,  $y$ -, and  $z$ -directions, respectively. The elastic moduli in 0° and 90° are  $E_{11}$  92 GPa and  $E_{22}$  8 GPa, respectively; in-plane shear modulus, Poisson’s ratio, and material density are  $E_{12}$  2.9 GPa,  $\nu_{12}$  0.33, and  $\rho$  1400 Kg $m^{-3}$ , respectively. A square “breathing” delamination is modeled between the interfaces of the first and second plies (0.625 mm in depth from the upper surface of the laminate). The delamination is centered at  $x=50$  mm and  $y=150$  mm. The area of the delamination is 40 mm × 40 mm, that amounts to 4% of the surface area of the laminate.

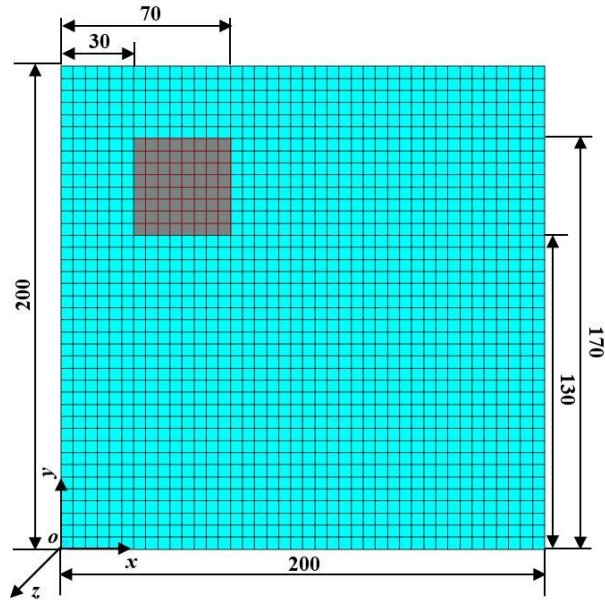


**Fig. 2.** FE model of delaminated CFRP laminate with dimensions in millimeters (the delamination is modeled between the interfaces of the first and second plies).

Note that, although delaminations are usually numerically and experimentally simulated in ellipse or circle shapes [44,45] to simulate practical delamination caused by external effects such as impacts and heats, in this study the delaminations are modeled in rectangular shapes, merely to simulate human-made delamination defects that were caused when the laminates were fabricated, which correspond to the delaminations manufactured by inserting square Teflon sheets between plies [46,47].

The composite laminate is modeled by the FE software ANSYS with 8-node hexahedron elements having the dimensions of  $5 \text{ mm} \times 5 \text{ mm} \times 0.625 \text{ mm}$  in the  $x$ -,  $y$ -, and  $z$ -directions, respectively. On the upper and lower delamination interfaces, coincident nodes in adjacent but separated elements are distributed. Note that contact elements are introduced between the upper and lower delamination interfaces [44,46], whereby the upper and lower delaminated layers are allowed to separate but not to penetrate into each other. Contact forces in the delamination are generated by virtual springs between the delamination interfaces using the penalty algorithm in ANSYS. For

this lightly-damped laminate, the damping ratio  $\xi = 0.1$  is considered according to the Rayleigh damping:

$$\xi = \frac{\tilde{\alpha}}{2\omega} + \frac{\tilde{\beta}\omega}{2}, \quad (24)$$

where  $\tilde{\alpha}$  and  $\tilde{\beta}$  are stiffness and mass damping parameters, respectively.

### 3.2 Nonlinear vibration subject to coupled vibro-acoustic excitation

To simulate the high-frequency acoustic excitation generated by a lead-zirconate-titanate (PZT) actuator, a harmonic concentrated force at 20 kHz is applied close to the middle of the upper edge of the upper surface; simultaneously, to simulate low-frequency vibration excitation generated by an electromechanical shaker, a harmonic concentrated force at 4500 Hz is applied in the geometrical center of the upper surface (labeled as excitation pattern I and illustrated in Fig. 3(a)).

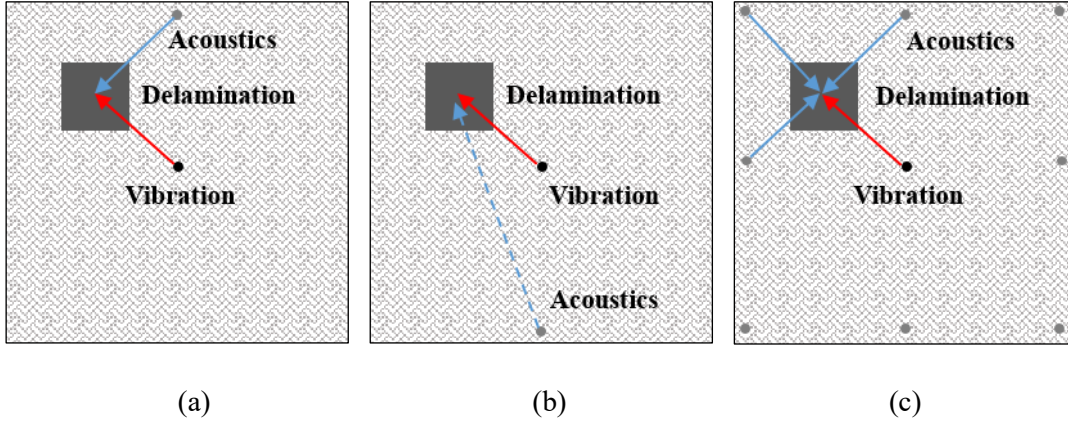


**Fig. 3.** Coupled vibro-acoustic excitation patterns (a) I (the delamination region is close to the acoustic excitation location), (b) II (the delamination region is distant from the acoustic excitation location), and (c) III (the array of coupled vibro-acoustic excitation applies to the laminate).

The amplitudes of the acoustic excitations are 1 N and the amplitude of the vibration excitation is 5 N. The time step is set to be one-tenth of the acoustic excitation

period for a wide range of frequency spectra, *i.e.*, five times  $\omega_H$ . Subject to coupled vibro-acoustic excitation, time histories of the steady-state displacement, velocity, and acceleration responses are extracted from the nodes on the lower surface of the laminate, as shown in Fig. 4. Correspondingly, their counterparts in the frequency domain are obtained by the fast Fourier transform (FFT), shown in Fig. 5 (abscissas are normalized by dividing by  $\omega_H$ ). It can be seen from Fig. 5 that the harmonic at  $\omega_L$  dominates the displacement, whereas the harmonic at  $\omega_H$  can be barely perceived. For the velocity response, weak nonlinear harmonics at  $\omega_H$  with small amplitudes appear in the frequency domain. In the acceleration response, besides the harmonic at  $\omega_L$ , evident harmonics appear at higher frequencies. The reason for the enhancement of harmonics can clearly be seen from differentiating relationships as follows:

$$\begin{aligned}
v = & -\sum_{m=1}^M \omega_{L,m} W_{L,m} \sin(\omega_{L,m} t + \phi_{L,m}) - \sum_{n=1}^N \omega_{H,n} W_{H,n} \sin(\omega_{H,n} t + \phi_{H,n}) \\
& - \sum_{n=1}^N \sum_{m=1}^M \omega_{Sn,\pm m} W_{Sn,\pm m} \sin(\omega_{Sn,\pm m} t + \phi_{Sn,\pm m}).
\end{aligned} \tag{25a}$$

$$\begin{aligned}
a = & -\sum_{m=1}^M \omega_{L,m}^2 W_{L,m} \cos(\omega_{L,m} t + \phi_{L,m}) - \sum_{n=1}^N \omega_{H,n}^2 W_{H,n} \cos(\omega_{H,n} t + \phi_{H,n}) \\
& - \sum_{n=1}^N \sum_{m=1}^M \omega_{Sn,\pm m}^2 W_{Sn,\pm m} \cos(\omega_{Sn,\pm m} t + \phi_{Sn,\pm m}).
\end{aligned} \tag{25b}$$

Equation (25a) indicates that each harmonic component in  $v$  is amplified by its frequency from  $W$  and Eq. (25b) indicates that each harmonic component in  $a$  is amplified by its frequency from  $v$ , which means that harmonics at higher frequencies can be amplified with larger amplitudes.

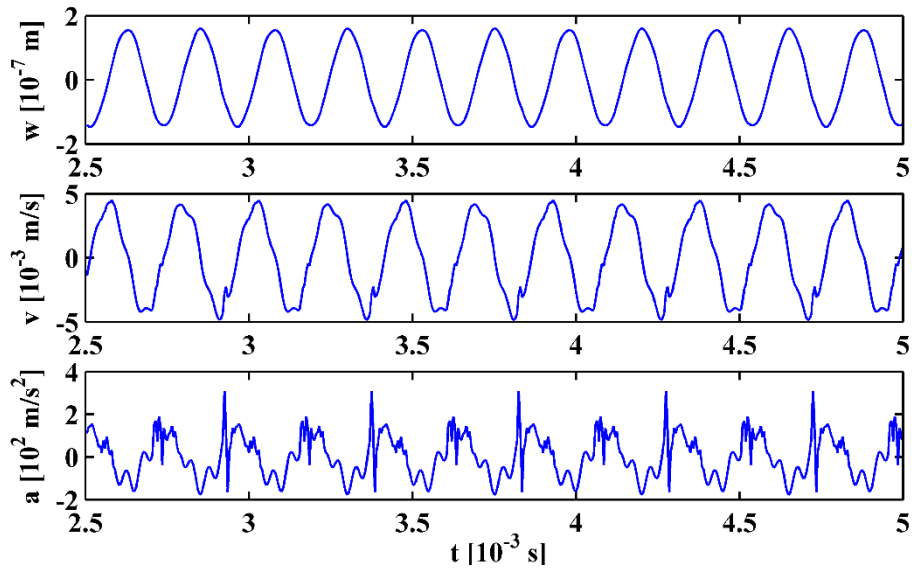


**Fig. 4.** Time histories of steady-state displacement ( $w$ ), velocity ( $v$ ), and acceleration ( $a$ ) responses (time histories of only 2.5 milliseconds are displayed).

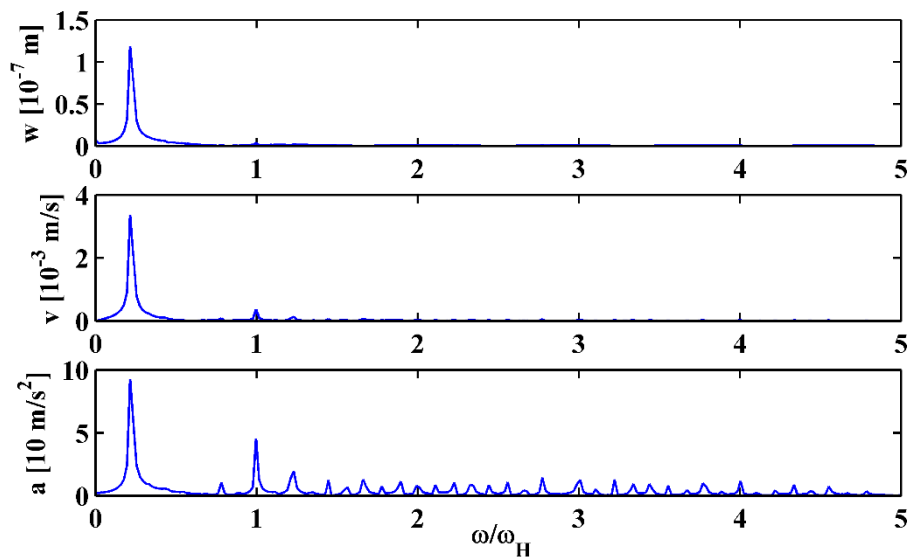


**Fig. 5.** Frequency spectra of steady-state displacement ( $w$ ), velocity ( $v$ ), and acceleration ( $a$ ) responses (abscissas are normalized by dividing by  $\omega_H$ ).

### 3.3 Array of coupled vibro-acoustic excitation

In the foregoing scenario with excitation pattern I, the delamination region is close to the acoustic excitation location (illustrated in Fig. 3(a)), such that high-frequency acoustic waves at  $\omega_H$  (indicated by the blue arrow) can propagate and interact with

the low-frequency vibration (indicated by the red arrow) in the delamination region, from the center of which the acceleration response in the frequency domain is shown in Fig. 6(a). However, when the delamination region is distant from the acoustic excitation location (labeled as excitation pattern II and illustrated in Fig. 3(b)), the harmonic at  $\omega_H$  and the nonlinear harmonics in the frequency domain are weakened with smaller amplitudes, as shown in Fig. 6(b). The mechanism of this phenomenon can be explained by Eqs. (18) and (20): higher harmonics at  $\omega_{H,n}$  and sideband harmonics at  $\omega_{Sn,\pm m}$  are associated with linear harmonics at  $\omega_H$  whose amplitude  $W_H$  is determined mainly by the acoustic excitation. High-frequency acoustic waves attenuate when they propagate along the distance (indicated by the dashed arrow in Fig. 3(b)) from the acoustic excitation location to the delamination region. Accordingly, decreases in  $W_H$  lead to weakening in modulation between linear and nonlinear harmonics. Therefore, the differences of intensities of nonlinear harmonics occur between the frequency spectra in Fig. 6(a) and (b). By addressing the situation that prior knowledge of the delamination region is usually absent in practical scenarios, this study proposes an array of coupled vibro-acoustic excitation to avoid wave attenuation of acoustic excitations. Thereby, vibration and acoustics can interact in the “breathing” delamination to generate nonlinear harmonics. Four acoustic excitation actuators are placed in the four corners of the surface and four other actuators are placed in the centers of four edges [48] (labeled as excitation pattern III and illustrated in Fig. 3(c)), such that there are always some acoustic sources near the delamination region, with the result that high-frequency acoustic waves at  $\omega_H$  can steadily propagate to the delamination region. In this condition, the acceleration response in the frequency domain is shown in Fig. 6(c), where the nonlinear harmonics are enhanced with amplified amplitudes.

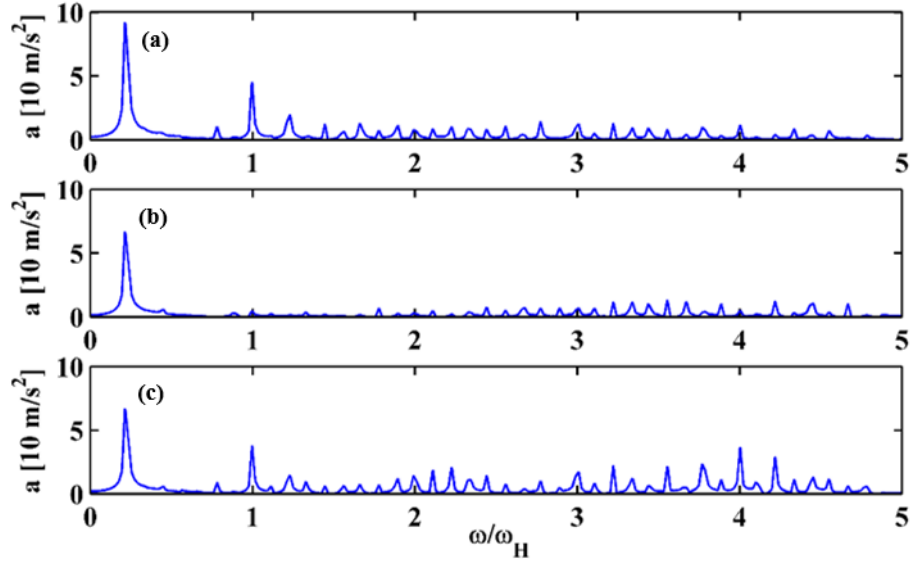


**Fig. 6.** Frequency spectra of steady-state acceleration responses with coupled vibro-acoustic excitation patterns (a) I (the delamination region is close to the acoustic excitation location), (b) II (the delamination region is distant from the acoustic excitation location), and (c) III (the array of coupled vibro-acoustic excitation is used).

To clearly demonstrate the nonlinear harmonics, higher harmonics are marked by circles and sideband harmonics are marked by triangles in Fig. 7, whose frequencies correspond to the theoretical values obtained by Eqs. (17b), (19b), and (21b), respectively. Figure 8 shows time histories of the steady-state displacement from the coincident nodes in the center of the upper (blue) and lower (red) delamination interfaces, in which “breathing” periods marked between dashed lines are found to be  $2\pi/\omega_L$  and  $2\pi/\omega_H$ , in agreement with the assumption in Section 2 that the “breathing” frequency can be  $\omega_L$  and  $\omega_H$ .

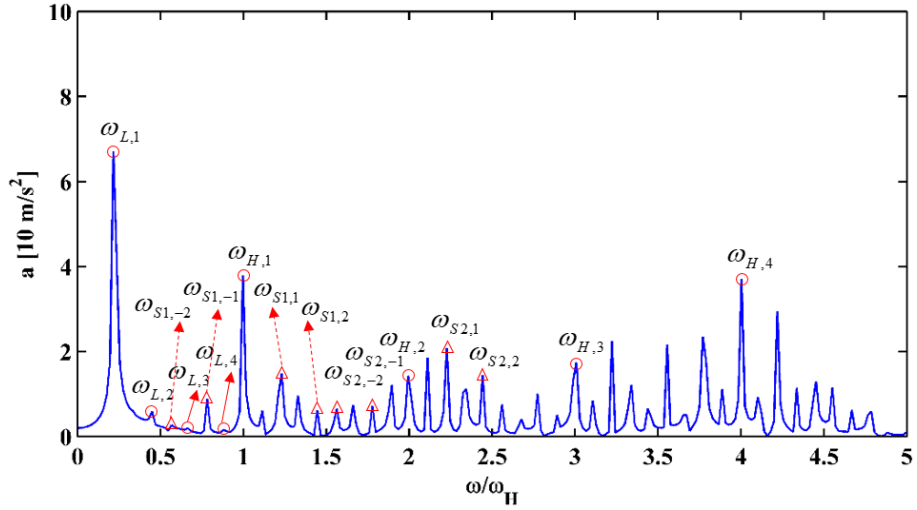


**Fig. 7.** Frequency spectrum of steady-state acceleration response with the array of coupled vibro-acoustic excitation (higher harmonics are marked by circles and sideband harmonics are marked by triangles).

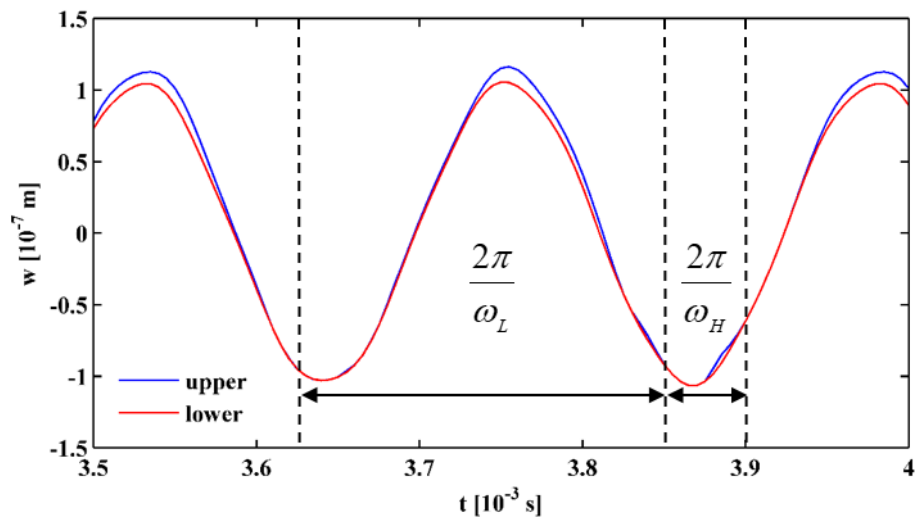
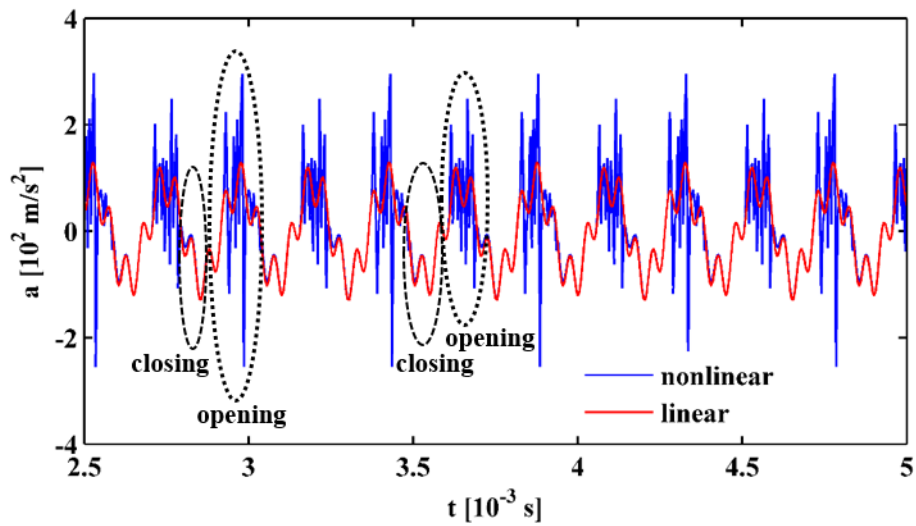


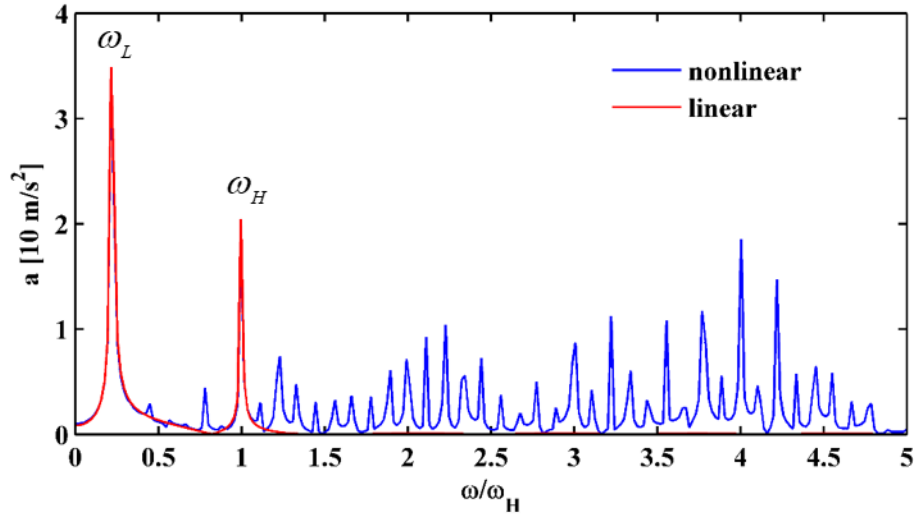
**Fig. 8.** Time histories of steady-state displacement responses from nodes in the middle of the upper (blue) and lower (red) delamination interface (“breathing” periods  $2\pi/\omega_L$  and  $2\pi/\omega_H$  are marked by dashed lines).

To show the differences between responses of laminates with respective “breathing” and open delamination, contact elements between the delamination interfaces are

removed from the FE model, whereby the “breathing” delamination degenerates into the open delamination. The nonlinear and linear steady-state acceleration responses of laminates with respective “breathing” (blue) and open (red) delamination are shown in Fig. 9(a). It can be seen from Fig. 9(a) that periodical differences appear between time histories, indicating that nonlinear and linear vibration responses gradually coincide during the process of delamination closing (marked by dashed ellipses), whereas they gradually separate during the process of delamination opening (marked by dotted ellipses). With transformation into the frequency domain by FFT, it can be seen from Fig. 9(b) that in nonlinear and linear responses, the amplitudes of linear harmonics at  $\omega_L$  and  $\omega_H$  almost coincide, whereas extra nonlinear harmonics appear for the nonlinear vibration. In a physical sense, it is reasonable to infer that the contact force between the “breathing” delamination interfaces is the intrinsic factor to cause nonlinear harmonics, in accord with the CAN theory [15].



(a)



(b)

**Fig. 9.** (a) Time histories of nonlinear (blue) and linear (red) steady-state acceleration responses, where closing and opening states of delamination are marked by dashed and dotted ellipses, respectively; (b) frequency spectra of nonlinear and linear steady-state acceleration responses (note that for nonlinear and linear responses, their amplitudes of linear harmonics at  $\omega_L$  and  $\omega_H$  almost coincide).

#### 4. Application in localization of “breathing” delamination

Recently, novel approaches relying on dynamic characteristics such as natural frequencies and mode shapes have been developed for locating structural damage, by which barely invisible delamination in composite laminates can be located [49-60]. Superior to nonlinear harmonics in frequency spectra that can manifest only the occurrence of delamination, ODSs of composite laminates used in this study are capable of locating delamination.

##### 4.1 Localization of “breathing” delamination using ODSs

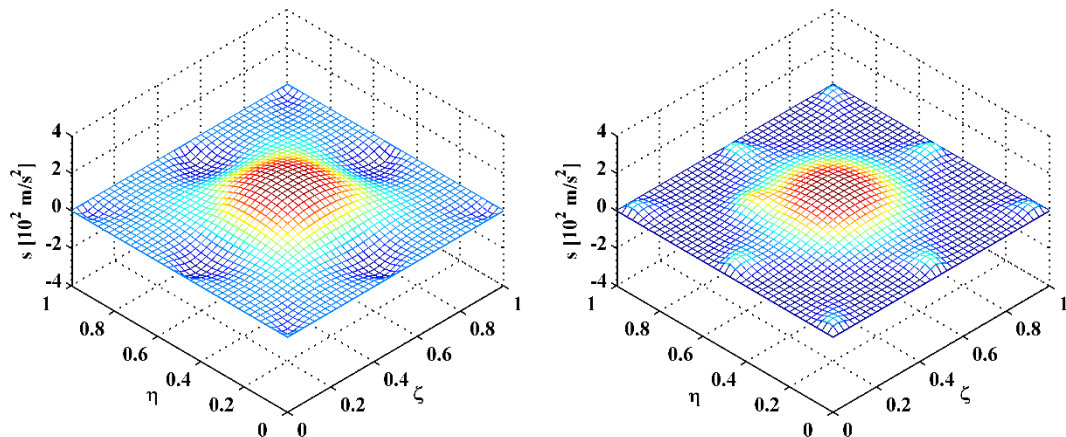
ODSs can be defined in both time and frequency domains [61]. In the time domain,  $w_{(p,q)}(t)$  denotes the steady-state acceleration response from the measurement point  $(p, q)$  at the specific time  $t$ ; correspondingly, in the frequency domain,  $\hat{w}_{(p,q)}(\omega)$  is the acceleration at the specific frequency  $\omega$ . As expressed in Eq. (26a), an ODS in

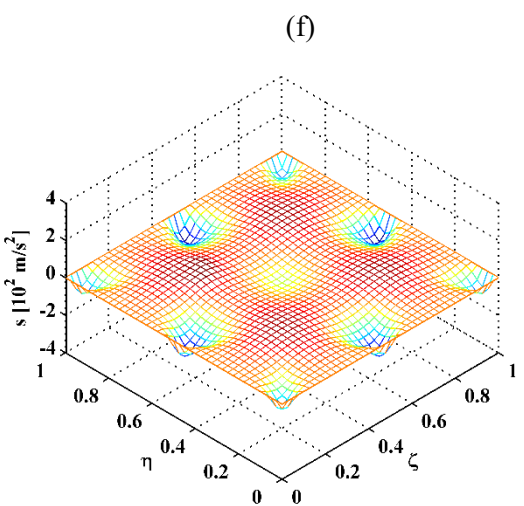
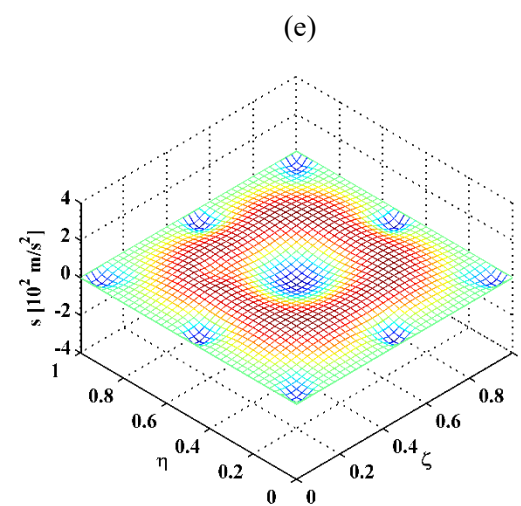
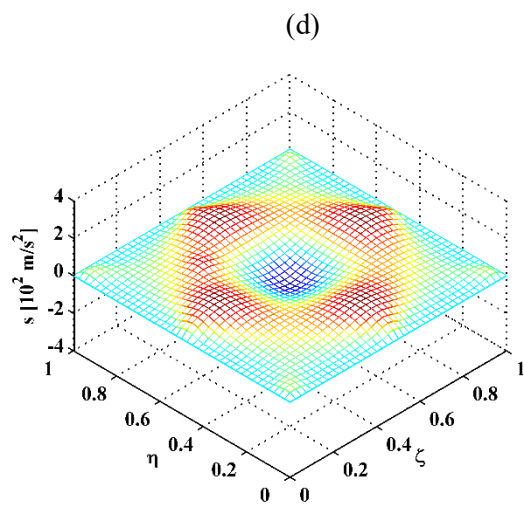
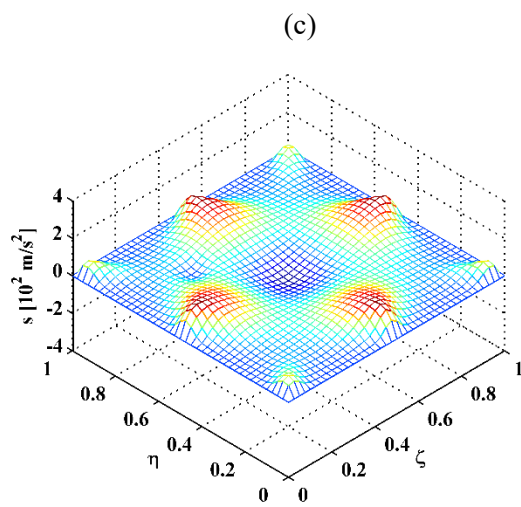
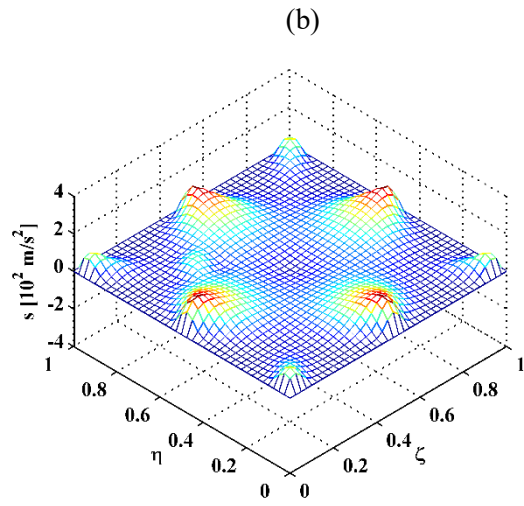
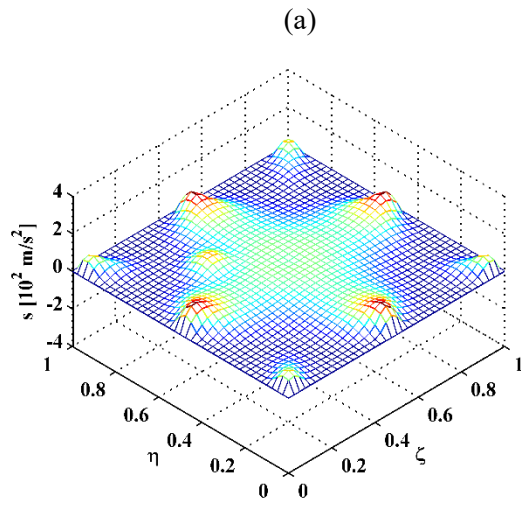
the time domain, denoted as  $s(t)$ , is constituted by  $w_{(p,q)}(t)$  with  $p=1,2,\dots,P$  and  $q=1,2,\dots,Q$ ; correspondingly, an ODS in the frequency domain, denoted as  $S(\omega)$ , is constituted by  $\hat{w}_{(p,q)}(\omega)$ . It is noteworthy that because  $S(\omega)$  is complex due to the FFT, its real or imaginary parts with larger amplitudes can be used to represent the ODS for a higher signal-to-noise ratio (SNR) [62,63].

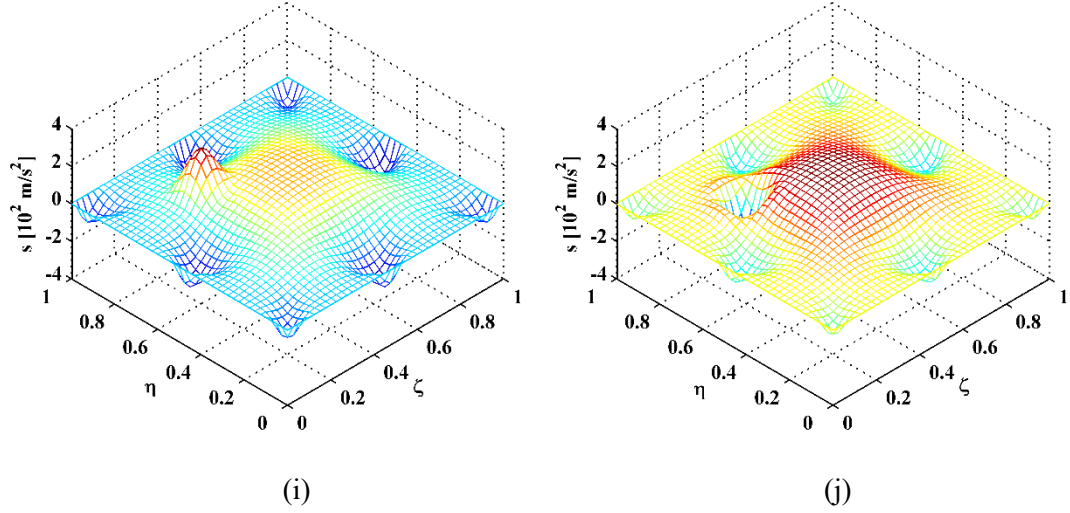
$$s(t) = \begin{bmatrix} w_{(1,1)}(t) & w_{(1,2)}(t) & \vdots & w_{(1,Q-1)}(t) & w_{(1,Q)}(t) \\ w_{(2,1)}(t) & \vdots & \vdots & \vdots & w_{(2,Q)}(t) \\ \vdots & \vdots & w_{(p,q)}(t) & \vdots & \vdots \\ w_{(P-1,1)}(t) & \vdots & \vdots & \vdots & w_{(P-1,Q)}(t) \\ w_{(P,1)}(t) & w_{(P,2)}(t) & \vdots & w_{(P,Q-1)}(t) & w_{(P,Q)}(t) \end{bmatrix}, \quad (26a)$$

$$S(\omega) = \begin{bmatrix} \hat{w}_{(1,1)}(\omega) & \hat{w}_{(1,2)}(\omega) & \vdots & \hat{w}_{(1,Q-1)}(\omega) & \hat{w}_{(1,Q)}(\omega) \\ \hat{w}_{(2,1)}(\omega) & \vdots & \vdots & \vdots & \hat{w}_{(2,Q)}(\omega) \\ \vdots & \vdots & \hat{w}_{(p,q)}(\omega) & \vdots & \vdots \\ \hat{w}_{(P-1,1)}(\omega) & \vdots & \vdots & \vdots & \hat{w}_{(P-1,Q)}(\omega) \\ \hat{w}_{(P,1)}(\omega) & \hat{w}_{(P,2)}(\omega) & \vdots & \hat{w}_{(P,Q-1)}(\omega) & \hat{w}_{(P,Q)}(\omega) \end{bmatrix}, \quad (26b)$$

By Eq. (26a), the ODSs in the time domain are extracted from the displacements of the nodes on the lower surface of the laminate. Figure 10(a) to (j) show ODSs at ten successive time steps in a period of  $2\pi / \omega_H$ . The results show that external excitations cause local deformations of the laminate; meanwhile, the NPF leads to local changes in the delamination region.



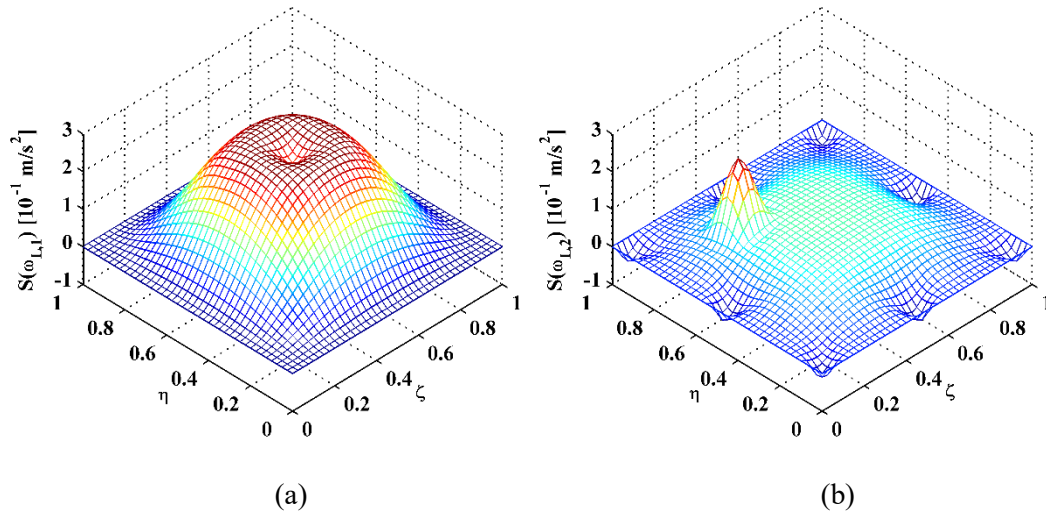


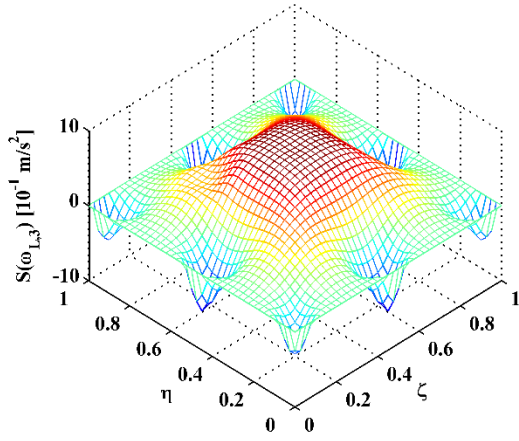


**Fig. 10.** ODSs in ten successive time steps (from (a) to (j)) in a period  $2\pi/\omega_H$ .

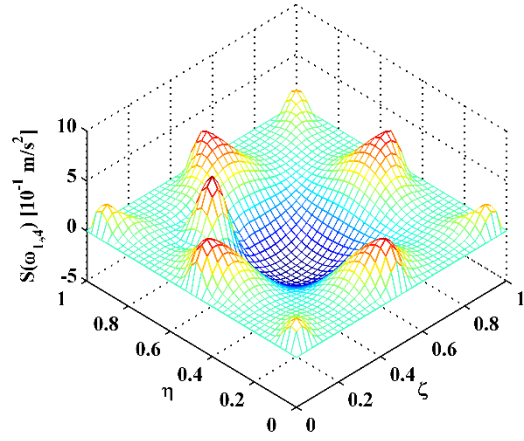
ODSs at linear harmonics are dominated by external excitations and local changes in the delamination region are likely to be obscured by the fluctuant trends produced by the external excitations. Contrastively, ODSs at nonlinear harmonics are totally determined by NPF that applies in the delamination region only. Therefore, local changes in the delamination region can be evidence for localization of delamination. By Eq. (26b), the ODSs in the frequency domain are extracted from the displacements of the nodes on the lower surface of the laminate. The ODSs associated with the low-frequency excitation ( $\omega_{L,1}$ ) and its 2nd ( $\omega_{L,2}$ ), 3rd ( $\omega_{L,3}$ ), and 4th ( $\omega_{L,4}$ ) higher harmonics are shown in Fig. 11(a), (b), (c), and (d), respectively. It can be seen from Fig. 11(a) that the ODS at  $\omega_{L,1}$  is dominated by the low-frequency excitation at  $\omega_L$  and the local change in the delamination region can be barely observed; in Fig. 11(b), the change in the delamination region stands out in the ODS at higher harmonic  $\omega_{L,2}$ , manifesting the occurrence of the delamination, and local changes in the excitation locations also appear, because the ODS at  $\omega_{L,2}$  is affected by linear harmonics at both

$\omega_{L,1}$  and  $\omega_{H,1}$  (as can be seen in Fig. 6); in Fig. 11(c) and (d), the changes in the delamination region become less pronounced because the ODSs are affected by the high-frequency excitation at  $\omega_H$ . Figure 12(a), (b), (c), and (d) show ODSs associated with high-frequency excitation at  $\omega_H$  and its 2nd ( $\omega_{H,2}$ ), 3rd ( $\omega_{H,3}$ ), and 4th ( $\omega_{H,4}$ ) higher harmonics, respectively. In Fig. 12(a), the ODS at  $\omega_{H,1}$  is dominated by the high-frequency excitation at  $\omega_H$  and the local change in the delamination region can be barely observed, similar to the result shown in Fig. 11(a). However, in the ODSs at higher harmonics  $\omega_{H,2}$ ,  $\omega_{H,3}$ , and  $\omega_{H,4}$ , the changes in the delamination region rise sharply, whereas deformations of the laminate outside the delamination region almost vanish. In practical applications, however, such high frequencies are likely to exceed the sampling frequency limitations of most conventional sensors such as accelerometers.



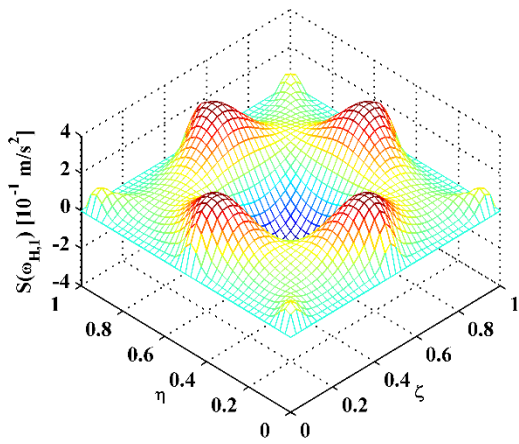


(c)

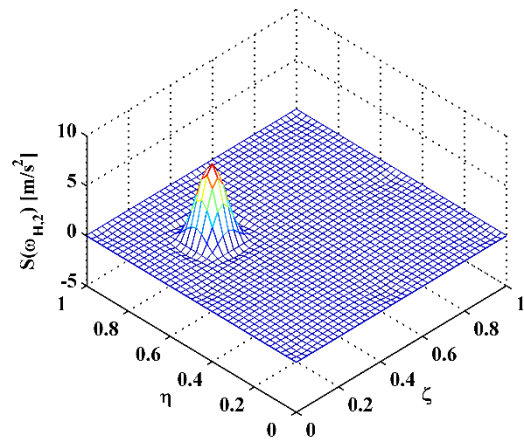


(d)

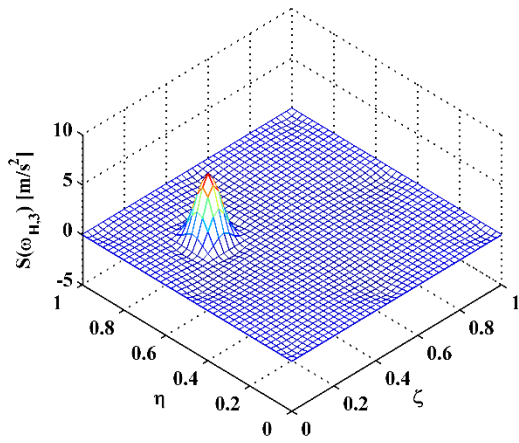
**Fig. 11.** ODSs at (a)  $\omega_{L,1}$  and its (b) 2nd, (c) 3rd, and (d) 4th higher harmonics at  $\omega_{L,2}$ ,  $\omega_{L,3}$ , and  $\omega_{L,4}$ , respectively.



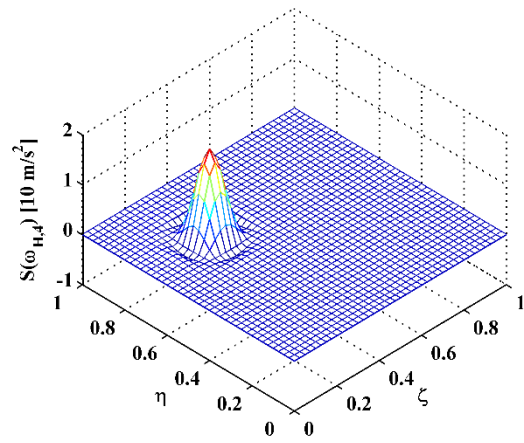
(a)



(b)



(c)



(d)

**Fig. 12.** ODSs at (a)  $\omega_{H,1}$  and its (b) 2nd, (c) 3rd, and (d) 4th higher harmonics at  $\omega_{H,2}$ ,  $\omega_{H,3}$ , and  $\omega_{H,4}$ , respectively.

ODSs at the -2nd (at  $\omega_{S1,-2}$ ), -1st (at  $\omega_{S1,-1}$ ), 1st (at  $\omega_{S1,1}$ ), and 2nd (at  $\omega_{S1,2}$ ) sideband harmonics of the harmonic at  $\omega_{H,1}$  are shown in Fig. 13(a), (b), (c), and (d), respectively. In Fig. 13(a), the ODS at the -2nd sideband harmonic is largely affected by the external excitations at  $\omega_L$  and  $\omega_H$ , with the result that the local change in the delamination region become less pronounced; in Fig. 13(b), the -1st sideband harmonic is not close to either  $\omega_L$  or  $\omega_H$ , and evident local change appears in the delamination region; in Fig. 13(c) and (d), the 1st and 2nd sideband harmonics are affected by the high-frequency excitation at  $\omega_H$ . Thereby, ODSs at sideband harmonics of the harmonic at  $\omega_{H,1}$  can be affected by linear harmonics. With this concern, sideband harmonics of the harmonic at  $\omega_{H,2}$  are selected to remove this effect; in addition,  $\omega_{H,2}$  can be within the sampling frequency limitations of sensors. It can be seen from Fig. 14 that ODSs at the -2nd (at  $\omega_{S2,-2}$ ), -1st (at  $\omega_{S2,-1}$ ), 1st (at  $\omega_{S2,1}$ ), and 2nd (at  $\omega_{S2,2}$ ) sideband harmonics of the harmonic at  $\omega_{H,2}$  show evident peaks in the delamination region, whereas deformations in other places are much less pronounced. Thus, ODSs at sideband harmonics of the harmonic at  $\omega_{H,2}$  have the capability for locating delamination of composite laminates. It is noteworthy that with the aid of advanced non-contact measurement technologies through non-contact vibration measurement techniques such as digital imaging and laser scanning, high accuracy and

spatial resolution of ODSs can become available for locating small “breathing” delamination.

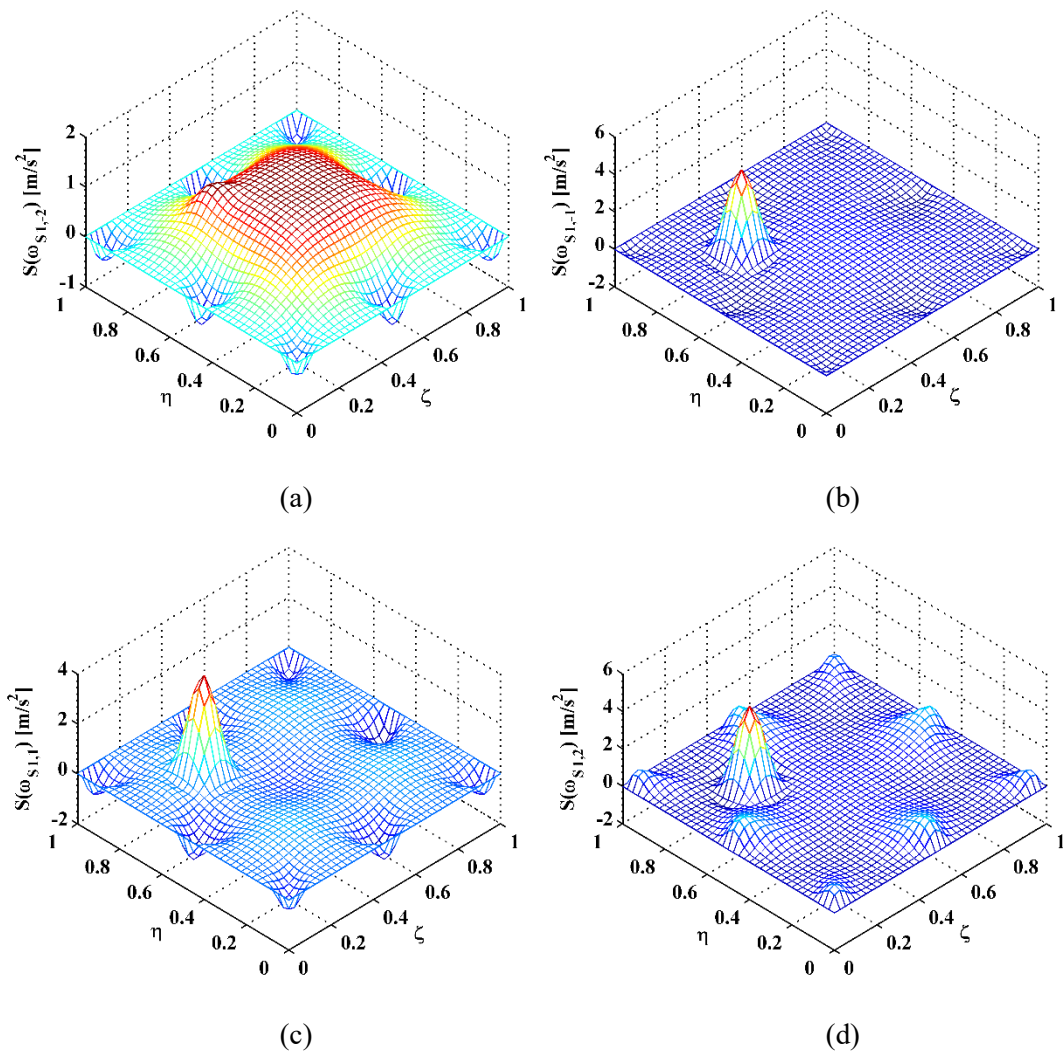


**Fig. 13.** ODSs at the (a) -2nd, (b) -1st, (c) 1st, and (d) 2nd sideband harmonics at  $\omega_{S1,-2}$ ,

$\omega_{S1,-1}$ ,  $\omega_{S1,1}$ , and  $\omega_{S1,2}$ , respectively.

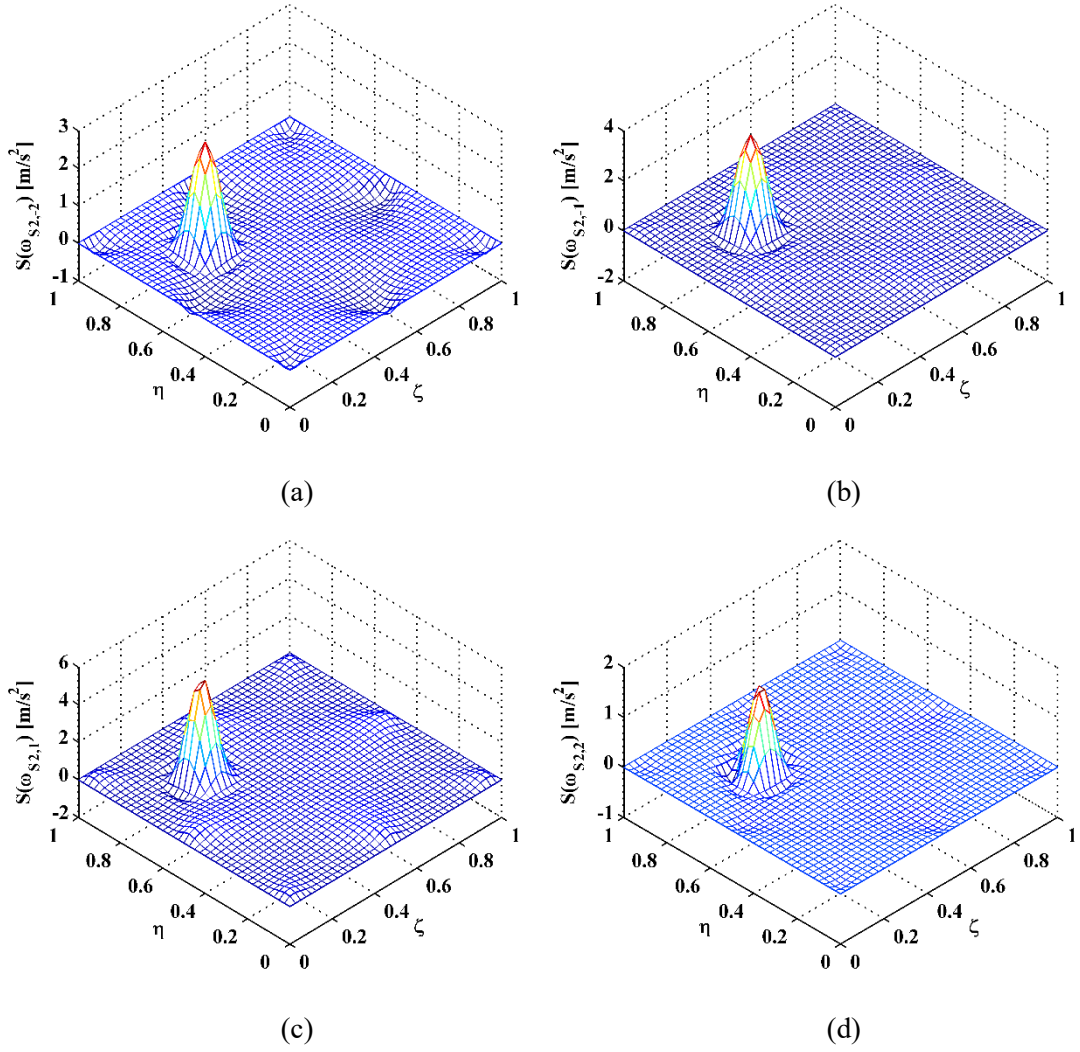


**Fig. 14.** ODSs at the (a) -2nd, (b) -1st, (c) 1st, and (d) 2nd sideband harmonics at  $\omega_{s_{2,-2}}$ ,

$\omega_{s_{2,-1}}$ ,  $\omega_{s_{2,1}}$ , and  $\omega_{s_{2,2}}$ , respectively.

## 4.2 Boundary effect on ODSs

In the foregoing scenarios, only the C-C-C-C (C for clamped) boundary condition was discussed. To validate the feasibility of ODSs in locating delamination with other boundary conditions, another three common boundary conditions are considered, F-F-F-F, S-S-S-S, and C-F-F-F (F for free and S for simply supported). Subject to the coupled vibro-acoustic excitation, time histories of the steady-state acceleration responses with F-F-F-F, S-S-S-S, and C-F-F-F boundary conditions are obtained, and shown in Fig. 15(a), (b), and (c), respectively. It can be seen from Fig. 15 that the

distributions of harmonics in frequency spectra are clearly affected by boundary conditions.

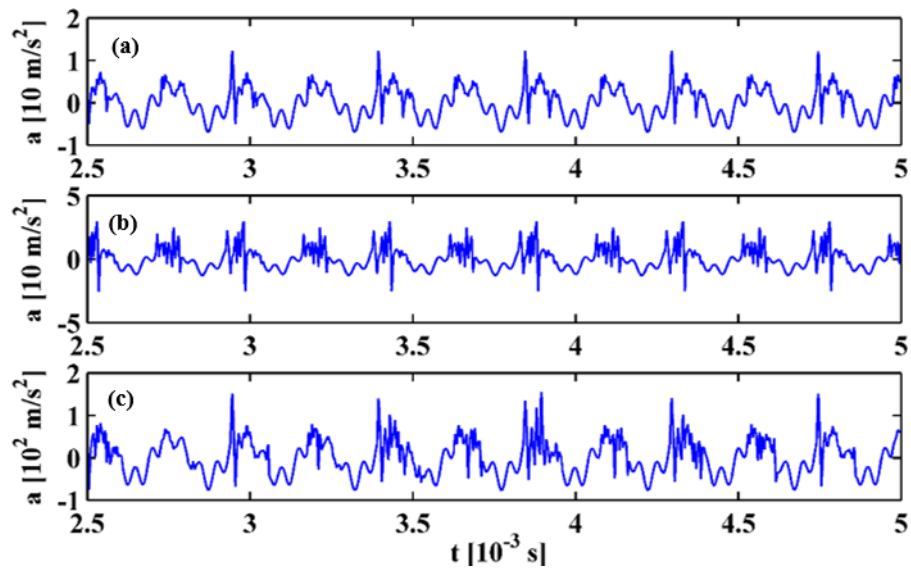


**Fig. 15.** Time histories of steady-state acceleration responses with (a) F-F-F-F, (b) S-S-S-S, and (c) C-F-F-F boundary conditions, respectively (time histories of only 2.5 milliseconds are displayed).

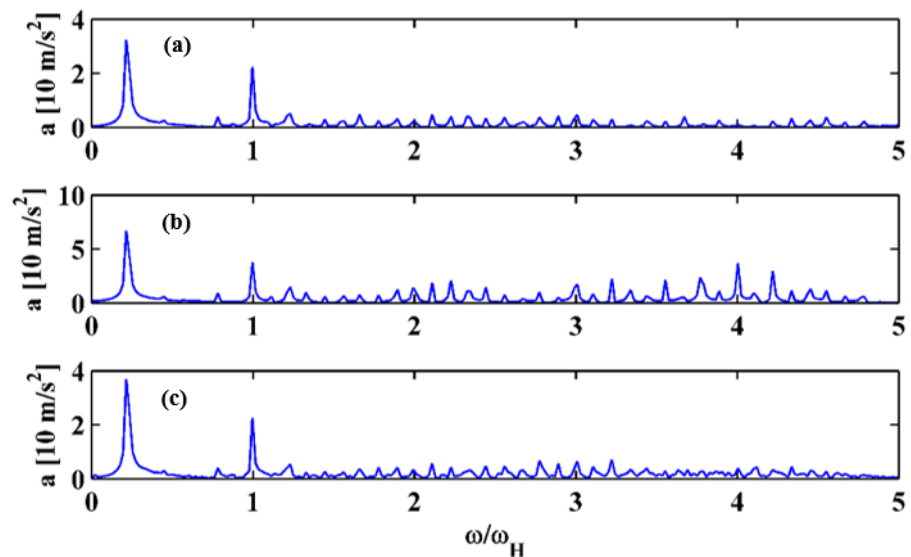


**Fig. 16.** Steady-state acceleration responses in frequency spectra with (a) F-F-F-F, (b) S-S-S-S, and (c) C-F-F-F boundary conditions, respectively.

The ODSs at the sideband harmonics of the harmonic at  $\omega_{H,2}$  with F-F-F-F, S-S-S-S, and C-F-F-F boundary conditions are obtained and are shown in Figs. 17, 18, and 19, respectively. It can be seen from the figures that fluctuant changes in the ODSs appear near free boundaries of the laminates, whereas such fluctuant changes vanish near the clamped or simply-supported edges, a finding that corresponds with the results in Fig. 14 with clamped boundaries. Therefore, clamped or simply-supported boundaries benefit locating “breathing” delamination.

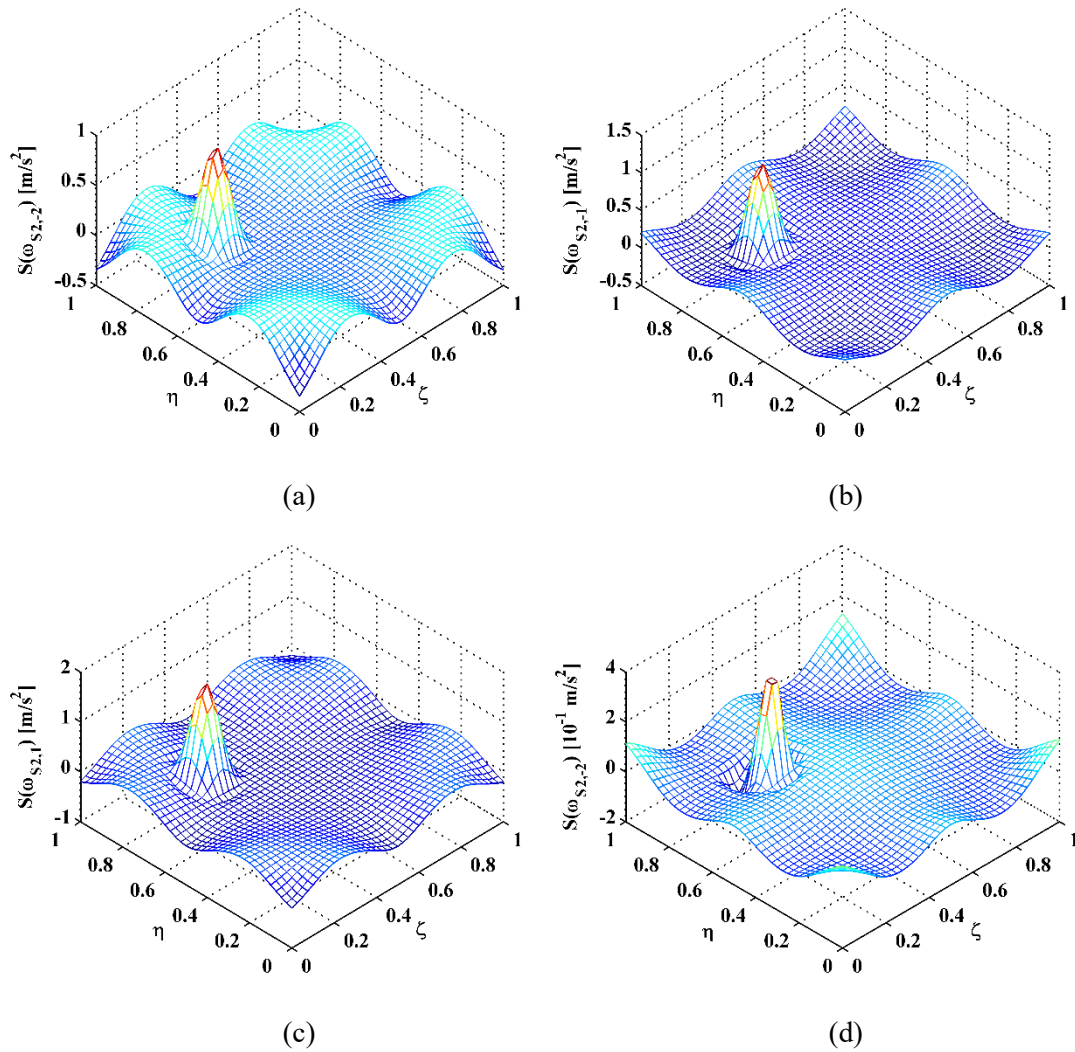
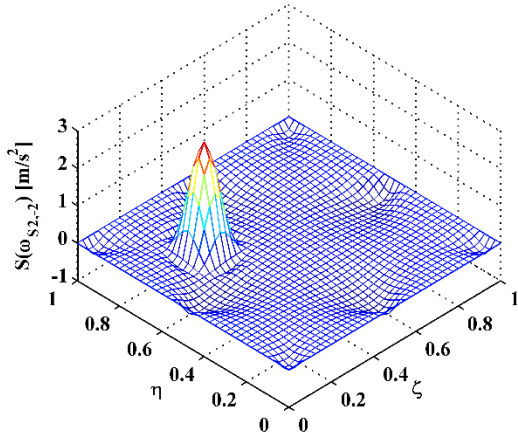
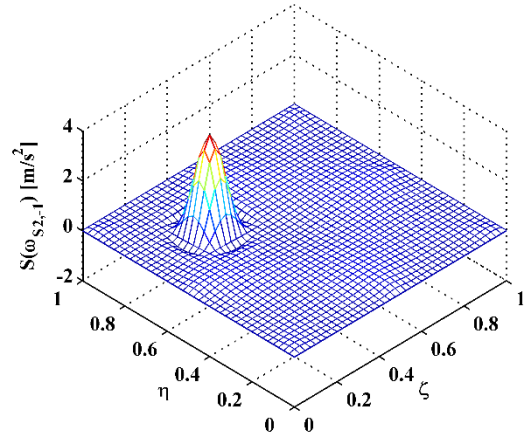


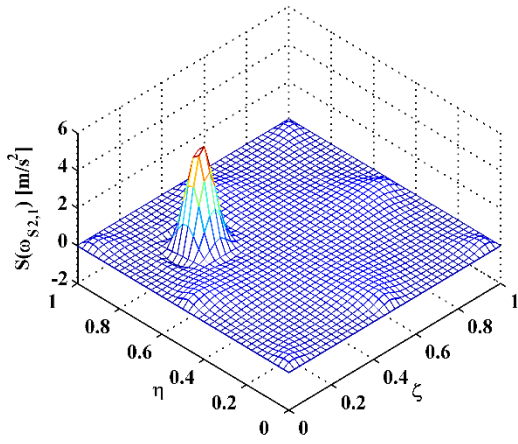
**Fig. 17.** ODSs (with F-F-F-F boundary conditions) at the (a) -2nd, (b) -1st, (c) 1st, and (d) 2nd sideband harmonics at  $\omega_{S2,-2}$ ,  $\omega_{S2,-1}$ ,  $\omega_{S2,1}$ , and  $\omega_{S2,2}$ , respectively.



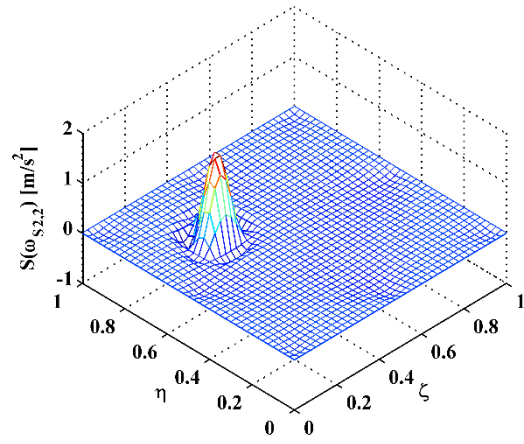
(a)



(b)

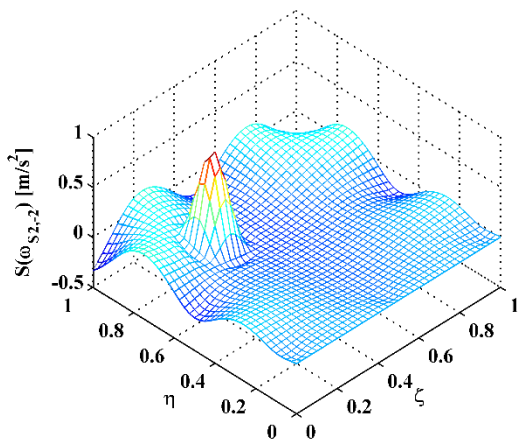


(c)

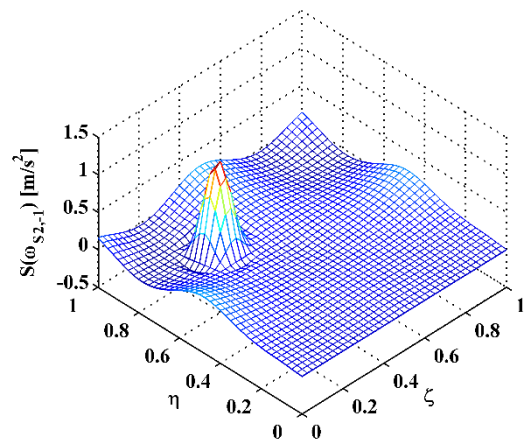


(d)

**Fig. 18.** ODSs (with S-S-S-S boundary conditions) at the (a) -2nd, (b) -1st, (c) 1st, and (d) 2nd sideband harmonics at  $\omega_{S2,-2}$ ,  $\omega_{S2,-1}$ ,  $\omega_{S2,1}$ , and  $\omega_{S2,2}$ , respectively.



(a)



(b)

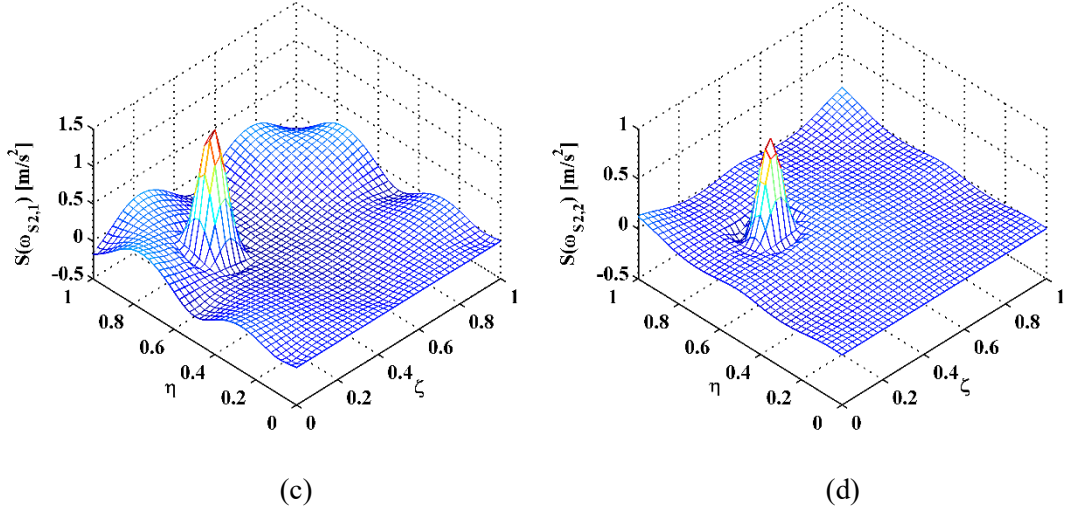


**Fig. 19.** ODSs (with C-F-F-F boundary conditions) at the (a) -2nd, (b) -1st, (c) 1st, and (d) 2nd sideband harmonics at  $\omega_{S2,-2}$ ,  $\omega_{S2,-1}$ ,  $\omega_{S2,1}$ , and  $\omega_{S2,2}$ , respectively.

From the findings in this study, it is noteworthy that with the aid of non-contact vibration measurement techniques such as digital imaging and laser scanning, vibration responses from measurement points on composite laminates can be acquired to formulate the ODSs in time and frequency domains by Eq. (26a) and (26b), respectively. As suggested by the numerical results, ODSs at sideband harmonics of the harmonic at  $\omega_{H,2}$  can be sensitive to “breathing” delamination, local changes of which can be used to locate the delamination. Nevertheless, this study focuses on the mechanism for generating nonlinear harmonics in “breathing” delamination. Numerical simulations using FE method are used to validate the mechanism and explore the application potential of the ODSs for locating delamination. Experimental tests in detection, localization, and quantitative evaluation of “breathing” delamination, as well as applications in real-world composite structures, can be addressed in a future study.

## 5. Concluding remarks

This study analytically formulates a new concept of NPF in “breathing” delaminations of composite laminates, by which the mechanism for generating nonlinear harmonics

by vibro-acoustic modulation is explicitly expounded. The nonlinear harmonics generated by “breathing” delaminations are numerically verified using the FE method. A novel approach using ODSs at nonlinear harmonics is proposed for locating “breathing” delaminations of composite laminates. Some conclusions are drawn as follows.

(1) The local stiffness in the delamination region changes periodically with the “breathing” motion of the delamination, which leads to the generation of the NPF in the delamination due to vibro-acoustic modulation. Components of the NPF are coupled with displacement components to reach a steady state, whereby nonlinear harmonics are generated.

(2) Subject to coupled vibro-acoustic excitation, the linear harmonics of a composite laminate bearing a “breathing” delamination are generated by the external excitations and the components of the NPF at linear harmonics, whereas nonlinear harmonics are totally generated by the NPF at nonlinear harmonics.

(3) High-frequency acoustic waves attenuate when they propagate in composite laminates. Addressing this problem, an array of coupled vibro-acoustic excitation is proposed to avoid wave attenuation of acoustic excitations. Thereby, vibration and acoustics can interact in “breathing” delaminations to generate nonlinear harmonics.

(4) ODSs at linear harmonics are dominated by external excitations and local changes in the delamination region are likely to be obscured by the fluctuant trends produced by the external excitations. In contrast, ODSs at nonlinear harmonics are totally determined by NPF that applies in the delamination region only. Therefore, local changes in the delamination region can be evidence of the localization of delamination.

## **Acknowledgments**

Wei Xu, Maosen Cao, and Zhongqing Su are grateful for the support from the National Natural Science Foundation of China through Grant Nos. 51708173, 11772115, and 51875492, respectively. This work is also partially supported by the China Postdoctoral Science Foundation (Nos. 2018T110433 and 2017M610289). Wei Xu is particularly grateful for the fellowship provided by the Hong Kong Scholars Program (No. XJ2018042).

## References:

- [1] Delia C, Shu D. Vibration of delaminated composite laminates: A review. *Applied Mechanics Reviews*, 2007; 60(1-6): 1-20.
- [2] Mujumdar P, Suryanarayan S. Flexural vibration of beams with delaminations. *Journal of Sound and Vibration*, 1998; 125: 441–461.
- [3] Lestari W, Hanagud S. Health monitoring of structures: Multiple delamination dynamics in composite beams. *Structural Dynamics and Materials Conference*, 1999, pp: 2453–2462.
- [4] Luo H, Hanagud S. Dynamics of delaminated beams. *International Journal of Solids and Structures*, 2000; 37(10): 1501-1519.
- [5] Wang J, Tong L. A study of the vibration of delaminated beams using a nonlinear anti-interpenetration constraint model. *Composite Structures*, 2002; 57: 483-488.
- [6] Andrews M, Massabo R. Delamination in flat sheet geometries with material imperfections and thickness variations. *Composites Part B-Engineering*, 2008; 39(1): 139-150.
- [7] Andrews M, Massabò R, Cavicchi A, Cox BN. Dynamic interaction effects of multiple delaminations in plates subject to cylindrical bending. *International Journal of Solids and Structures*, 2009; 46(9): 1815-1833.
- [8] Manoach E, Warminski J, Mitura A, Samborski S. Dynamics of a composite Timoshenko beam with delamination. *Mechanics Research Communications*, 2012; 46: 47-53.
- [9] Wang J, Liu Y, Gibby J. Vibration of split beams. *Journal of Sound and Vibration*, 1982; 84: 491–502.

- [10] Kundu T. Nonlinear Ultrasonic and Vibro-Acoustical Techniques for Nondestructive Evaluation, Taylor and Francis, 2019.
- [11] Zarembo L, Krasilnikov V, Sluch V, Serdobolskaya O. On some phenomena accompanying forced non-linear vibrations of acoustic resonators. *Akust. Zh.* 1966; 12: 486-487.
- [12] Solodov I. Ultrasonics of non-linear contacts: propagation, reflection and NDE-applications. *Ultrasonics*, 1998; 36(1-5): 383-390.
- [13] Van den Abeele K, Johnson P, Sutin A. Nonlinear elastic wave spectroscopy (NEWS) techniques to discern material damage, Part I: Nonlinear wave modulation spectroscopy (NWMS), *Research in Nondestructive Evaluation*, 2000; 12(1): 17-30.
- [14] Van den Abeele K, Carmeliet J, Ten Cate J, Johnson P. Nonlinear elastic wave spectroscopy (NEWS) techniques to discern material damage, Part II: Single-mode nonlinear resonance acoustic spectroscopy. *Research in Nondestructive Evaluation*, 2000; 12(1): 31-42.
- [15] Solodov I, Krohn N, Busse G. CAN: an example of nonclassical acoustic nonlinearity in solids. *Ultrasonics*, 2002; 40: 621-625.
- [16] Meo M, Zumpano G. Nonlinear elastic wave spectroscopy identification of impact damage on a sandwich plate. *Composite Structures*, 2005; 71(3-4): 469-474.
- [17] Lim H, Sohn H, Liu P, Binding conditions for nonlinear ultrasonic generation unifying wave propagation and vibration. *Applied Physics Letters*, 2014; 104: 214103.

- [18] Ciampa F, Scarselli G, Meo M. On the generation of nonlinear damage resonance intermodulation for elastic wave spectroscopy. *Journal of The Acoustical Society of America*, 2017; 141(4): 2364-2374.
- [19] Solodov I, Wackerl J, Pfleiderer K, Busse G. Nonlinear self-modulation and subharmonic acoustic spectroscopy for damage detection and location. *Applied Physics Letters*, 2004; 84(26): 5386-5388.
- [20] Solodov I, Busse G. Nonlinear air-coupled emission: The signature to reveal and image microdamage in solid materials. *Applied Physics Letters*, 2007; 91: 251910.
- [21] Meo M, Polimeno U, Zumpano G. Detecting damage in composite material using nonlinear elastic wave spectroscopy methods. *Applied Composite Materials*, 2008; 15(3): 115-126.
- [22] Polimeno U, Meo M. Detecting barely visible impact damage detection on aircraft composites structures. *Composite Structures*, 2009; 91: 398-402.
- [23] Aymerich F, Staszewski W. Impact damage detection in composite laminates using nonlinear acoustics. *Composites Part A-Applied Science and Manufacturing*, 2010; 41(9): 1084-1092.
- [24] Klepka A, Staszewski W, Di Maio D, Scarpa F. Impact damage detection in composite chiral sandwich panels using nonlinear vibro-acoustic modulations, *Smart Materials and Structures*. 2013; 22: 084011.
- [25] Klepka A, Pieczonka L, Staszewski W, Aymerich F. Impact damage detection in laminated composites by non-linear vibro-acoustic wave modulations. *Composites Part B-Engineering*, 2014; 65: 99-108.

- [26] Pieczonka L, Ukowski P, Klepka A, Staszewski W, Uhl T, Aymerich F. Impact damage detection in light composite sandwich panels using piezo-based nonlinear vibro-acoustic modulations. *Smart Materials and Structures*, 2014; 23: 105021.
- [27] Dionysopoulos D, Fierro G, Meo M, Ciampa F. Imaging of barely visible impact damage on a composite panel using nonlinear wave modulation thermography. *NDT & E International*, 2018; 95: 9-16.
- [28] Chrysochoidis N, Barouni A, Saravanous D. Delamination detection in composites using wave modulation spectroscopy with a novel active nonlinear acousto-ultrasonic piezoelectric sensor. *Journal of Intelligent Material Systems and Structures*, 2011; 22: 2193-2206.
- [29] Chen B, Soh S, Lee H, Tay T, Tan V. A vibro-acoustic modulation method for the detection of delamination and kissing bond in composites. *Journal of Composite Materials*, 2016; 50: 3089-3104.
- [30] Solodov I, Bai J, Bekgulyan S, Busse G. A local defect resonance to enhance acoustic wave-defect interaction in ultrasonic nondestructive evaluation. *Applied Physics Letters*, 2011; 99: 211911.
- [31] Leissa A, Qatu M. *Vibration of Continuous Systems*, 2011, McGraw Hill
- [32] Cao M, Su Z, Xu H, Radziński M, Xu W, Ostachowicz W. A novel damage characterization approach for laminated composites in the absence of material and structural information. *Mechanical Systems and Signal Processing*, 2020; 143: 106831.
- [33] Semperlotti F, Wang K, Smith E. Localization of a breathing crack using nonlinear

- subharmonic response signals. *Applied Physics Letters*, 2009; 95(25): 254101.
- [34] Semperlotti F, Wang K, Smith E. Localization of a breathing crack using superharmonic signals due to system nonlinearity. *AIAA Journal*, 2009; 47(9): 2076–2086.
- [35] Hu H, Staszewski W, Hu N, Jenal R, Qin G. Crack detection using nonlinear acoustics and piezoceramic transducers—instantaneous amplitude and frequency analysis. *Smart Materials and Structures*, 2010; 19(6): 065017.
- [36] Kim G, Johnson D, Semperlotti F, Wang K. Localization of breathing cracks using combination tone nonlinear response. *Smart Materials and Structures*, 2011; 20(5): 055014.
- [37] Klepka A, Staszewski W, Jenal R, Szwedo M, Iwaniec J, Uhl T. Nonlinear acoustics for fatigue crack detection—experimental investigations of vibroacoustic wave modulations. *Structural Health Monitoring-An International Journal*, 2011; 11(2): 197–211.
- [38] Asnaashari E, Sinha J. Development of residual operational deflection shape for crack detection in structures. *Mechanical Systems and Signal Processing*, 2014; 43(1-2): 113–123.
- [39] Bovsunovsky A, Surace C. Non-linearities in the vibrations of elastic structures with a closing crack: A state of the art review. *Mechanical Systems and Signal Processing*, 2015; 62-63: 129–148.
- [40] Broda D, Pieczonka L, Hiwarkar V, Staszewski W, Silberschmidt V. Generation of higher harmonics in longitudinal vibration of beams with breathing cracks. *Journal*

of Sound and Vibration, 2016; 381: 206–219.

- [41] Lu Z, Dong D, Ouyang H, Cao S, Hua C. Localization of breathing cracks in stepped rotors using super-harmonic characteristic deflection shapes based on singular value decomposition in frequency domain. *Fatigue and Fracture of Engineering Materials and Structures*, 2017; 40: 1825–1837.
- [42] Wang K, Fan Z, Su Z. Orienting fatigue cracks using contact acoustic nonlinearity in scattered plate waves. *Smart Materials and Structures*, 2018; 27: 09LT01.
- [43] Cheng S, Swamidas A, Wu X, Wallace W. Vibrational response of a beam with a breathing crack. *Journal of Sound and Vibration*, 1999; 225(1): 201-208.
- [44] Singh A, Chen B, Tan V, Tay T, Lee H. Finite element modeling of nonlinear acoustics/ultrasonics for the detection of closed delaminations in composites. *Ultrasonics*, 2017; 74: 89-98.
- [45] Li F, Meng G, Kageyama K, Su Z, Lin Y. Optimal mother wavelet selection for lamb wave analyses. *Journal of Intelligent Material Systems and Structures*, 2009; 20(10): 1147-1161.
- [46] Garcia D, Palazzetti R, Trendafilova I, Fiorini C, Zucchelli A. Vibration-based delamination diagnosis and modelling for composite laminate plates. *Composite Structures*, 2015; 130: 155-162.
- [47] Xu W, Cao M, Li X, Radziński M, Ostachowicz W, Bai R. Delamination monitoring in CFRP laminated plates under noisy conditions using complex-wavelet 2D curvature mode shapes. *Smart Material and Structures*, 2017; 26: 104008.

- [48] Su Z, Ye L. Lamb Wave Propagation-based Damage Identification for Quasi-isotropic CF/EP Composite Laminates Using Artificial Neural Algorithm: Part II - Implementation and Validation. *Journal of Intelligent Material Systems and Structures*, 2005; 16(2): 113-125.
- [49] Qiao P, Lu K, Lestari W, Wang J. Curvature mode shape-based damage detection in composite laminated plates. *Composite Structures*, 2007; 80: 409-428.
- [50] Araújo dos Santos J, Lopes H, Vaz M, Soares CM, Soares CA, De Freitas M. Damage localization in laminated composite plates using mode shapes measured by pulsed TV holography. *Composite Structures*, 2006; 76: 272-281
- [51] Wang Q, Wu N. Detecting the delamination location of a beam with a wavelet transform: an experimental study. *Smart Materials and Structures*, 2011; 20: 012002.
- [52] Solodov I, Busse G. Multi-frequency defect selective imaging via nonlinear ultrasound. *Acoustical Imaging 2012*; 31: 385-398.
- [53] Cao M, Ostachowicz W, Radziński M, Xu W. Multiscale shear-strain gradient for detecting delamination in composite laminates. *Applied Physics Letters*, 2013; 103: 101910
- [54] Pérez M, Gil L, Oller S. Impact damage identification in composite laminates using vibration testing. *Composite Structures*, 2014; 108: 267-276.
- [55] Zhang Z, He M, Liu A, Singh H, Ramakrishnan K, David H. Vibration-based assessment of delaminations in FRP composite plates. *Composites Part B: Engineering*, 2018; 144: 254-266.

- [56] Chen D, Xu Y, Zhu W. Non-model-based identification of delamination in laminated composite plates using a continuously scanning laser Doppler vibrometer system. *Journal of Vibration and Acoustics*, 2018; 140(4): 041001
- [57] Xu W, Fang H, Cao M, Zhou L, Wang Q, Ostachowicz W. A noise-robust damage indicator for characterizing singularity of mode shapes for incipient delamination identification in CFRP laminates. *Mechanical Systems and Signal Processing*, 2019; 121: 183-200.
- [58] Zhang Z, Pan J, Luo W, Ram K, Singh H. Vibration-based delamination detection in curved composite plates. *Composites Part A: Applied Science and Manufacturing*, 2019; 119: 261-274.
- [59] Péreza M, Serra-López R. A frequency domain-based correlation approach for structural assessment and damage identification. *Mechanical Systems and Signal Processing*, 2019; 119: 432-456.
- [60] Xu W, Su Z, Liu J, Cao M, Ostachowicz W. Singular energy component for identification of initial delamination in CFRP laminates through piezoelectric actuation and non-contact measurement. *Smart Materials and Structures*, 2020; 29: 045001.
- [61] Schwarz B, Richardson M. Introduction to operating deflection shapes. *CSI Reliability Week*, 1999; 10: 121–126.
- [62] Xu W, Zhu W, Smith S, Cao M. Structural damage detection using slopes of longitudinal vibration shapes. *Journal of Vibration and Acoustics*, 2016; 138(3): 034501.

[63] Xu W, Zhu W, Xu Y, Cao M, A comparative study on structural damage detection using derivatives of laser-measured flexural and longitudinal vibration shapes, *Journal of Nondestructive Evaluation*, 2020; 39: 59.